Chapter 11

Magma–water interactions

Ken Wohletz, Bernd Zimanowski and Ralf Büttner

Overview

Magma–water interaction is an unavoidable consequence of the hydrous nature of the Earth's crust, and may take place in environments ranging from submarine to desert regions, producing volcanic features ranging from passively effused lava to highly explosive events. Hydrovolcanism is the term that describes this interaction at or near the Earth's surface, and it encompasses the physical and chemical dynamics that determine the resulting intrusive or extrusive behavior, and the character of eruptive products and deposits. The development of physical theory describing the energetics and the hydrodynamics (dynamics of fluids and solids at high strain rates) of magma–water interaction relies on an understanding of the physics of water behavior in conditions of rapid heating, the physics of magma as a material of complex rheology, and the physics of the interaction between the two, as well as detailed field observations and interpretation of laboratory experiments. Of primary importance to address are the nature of heat exchange between the magma and water during interaction, the resulting fragmentation of the magma, and the constraints on system energetics predicted by equilibrium and non-equilibrium thermodynamics. Taken together, these approaches elucidate the relationships among aqueous environment, interaction physics, and eruptive phenomena and landforms.

11.1 Introduction: magma and the hydrosphere

The vast majority of volcanic eruptions take place under water because most volcanism concentrates at mid-oceanic ridges where new oceanic crust is produced. By definition, every kind of extrusive subaqueous volcanism on Earth is hydrovolcanic since some degree of water interaction must take place. The hydrosphere also exists in continental areas, as the consequence not only of lakes and rivers, but also of groundwater and hydrous fluids that circulate in joints and faults in the upper crust and fill pore space in sedimentary rocks. Such locations are typically referred to as geohydrological environments. As a consequence, subaerial volcanism is commonly influenced by magma–water interaction. Chapter 12 describes deep-sea eruptions in greater detail, whereas this chapter

Modeling Volcanic Processes: The Physics and Mathematics of Volcanism, eds. Sarah A. Fagents, Tracy K. P. Gregg, and Rosaly M. C. Lopes. Published by Cambridge University Press.

focuses on magma–water interaction in surface and near-surface environments.

The explosive intensity of volcanic eruptions depends on the extrusion rate of magma and on the coupling of its thermal energy (i.e., heat flux) to the surroundings. Because the thermal conductivity of magma is very low, hydrovolcanic heat flux is mainly governed by the size of the interfacial area between magma and water and its growth rate during interaction. Thus, the key process that determines the thermal energy flux from the magma to its surroundings is magma fragmentation.

Water is the predominant thermodynamic working fluid on Earth, and practically every power plant in the world uses water for converting thermal energy into mechanical energy and finally into electricity. Where rising magma contacts water (in contrast to rocks or atmospheric gases) the major effect is an increase in thermal energy flux and, by analogy to commercial power production, in the efficacy of heat and power generation. For this reason there is a rich technical literature in science and engineering that can be applied to understanding magma–water interactions; this is the intent of this chapter.

11.2 Hydrovolcanism: from pillow lava to maar tephra

11.2.1 History of hydrovolcanism

Magma–water interactions occur deep within the Earth (*hydromagmatism*) as well as at or near its surface (*hydrovolcanism*). These terms are roughly synonymous because in many cases the realm where interaction initiates and later manifests may span from deep within the Earth's crust to the surface. For this reason the term *phreatomagmatic* is used to designate interaction within the phreatic realm of the Earth's surface, which includes the zone of saturation where groundwater and surface water exist.

The topic of magma–water interaction may be considered to have its roots in the eighteenth-Century Neptunists' theory about the origin of basaltic rocks in oceans (which was later formalized by Abraham Werner). Initial ideas about the role of ground and surface water in volcanism developed during the last century. These perceptions resulted largely from observations of unusually explosive periods of Hawaiian volcanism, during which groundwater entered rifts along which normal lava fountaining had previously occurred (Jaggar, 1949), as well as through examination of fragmental basalts found where lava had entered water (Fuller, 1931). Three well-documented eruptions during the late 1950s and early 1960s brought an increased awareness of explosive hydrovolcanism: Capelinhos, Azores (Tazieff, 1958; Servicos Geologicos de Portugal, 1959), Surtsey, Iceland (Thorarinsson, 1964), and Taal, Philippines (Moore *et al.*, 1966). Fisher and Waters (1970), Waters and Fisher (1971), and Heiken (1971) expanded the characterization of phreatomagmatic eruptions to include steam-rich eruption columns, base surges, and typical landforms such as maars, tuff rings, and tuff cones. As a result of this work, numerous twentieth century phreatomagmatic eruptions are now recognized, many of which formed maar-like craters (e.g., Self *et al.*, 1980). After cinder cones, phreatomagmatic constructs (tuff rings, tuff cones, and maars) are perhaps the most abundant terrestrial volcanic landform. However, magma–water interaction is certainly not limited to explosive phreatomagmatic eruptions – the hydrologic environment plays a major role in determining the kind of interaction that can occur.

11.2.2 Hydrovolcanic environments

The wide variety of hydrovolcanic phenomena suggests that interaction between water and magma or magmatic heat may occur in any volcanic setting and geohydrological environment, and is not restricted to a particular magma composition. From the formation of pillow lava and lineated, folded, and jumbled sheet flows in deep water, to the intrusion of breccia in dikes and sills deep in the crust, to the eruption of plumes of fine ash in desert, tropical, and shallow water environments, magma–water interaction includes both passive and dynamic phenomena. During ascent to the surface, magma commonly encounters

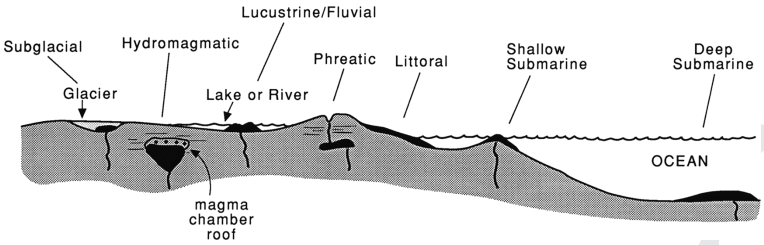

Figure 11.1 Schematic illustration of common environments of hydrovolcanism (adapted from Wohletz, 1993).

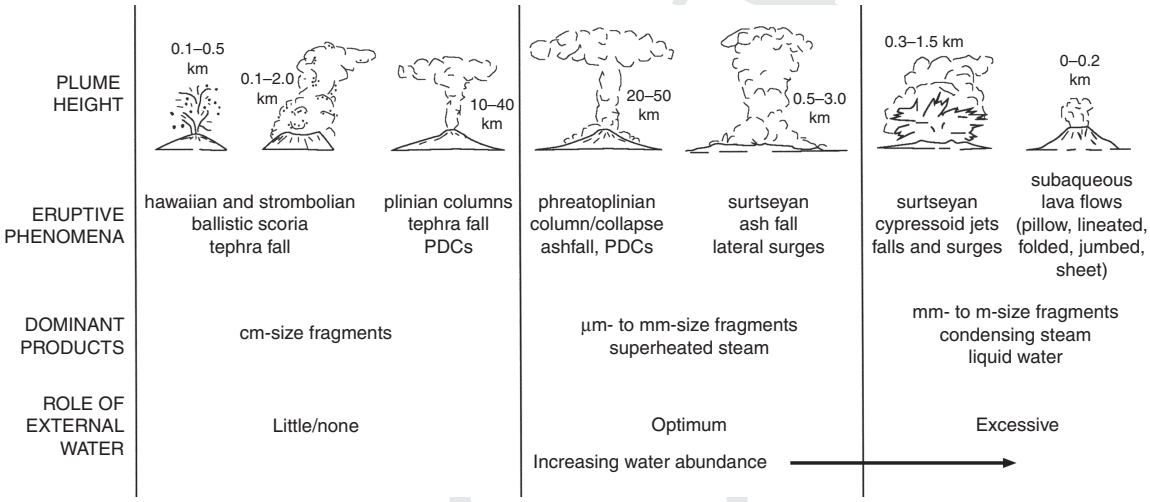

Figure 11.2 Relationship of typical eruptive phenomena and products to water abundance (adapted from Sheridan and Wohletz, 1983). Deposit features indicative of magma–water interaction may include planar to duneform bedding, impact sags or slumps and, particularly for greater water abundances, accretionary lapilli, soft sediment deformation structures, and cohesive, altered, or vesiculated tuff.

groundwater, connate (entrapped depositional) water, marine, fluvial, or lacustrine water, ice, or rain water (Fig. 11.1). From this diversity of hydrovolcanic environments comes a wide range of terminology. For example, the subaqueous environment includes all activity beneath a standing body of water (Kokelaar, 1986); products of this activity have been called *subaquatic* (Sigvaldason, 1968), *aquagene* (Carlisle, 1963), *hyaloclastite* (for deep marine; Bonatti, 1976), *hyalotuff* (for shallow marine; Honnorez and Kirst, 1975), and *littoral* (Wentworth, 1938). Volcanism that heats groundwater to produce steam explosions that do not eject juvenile magma fragments is called *phreatic* (Ollier, 1974) or *hydrothermal* (Muffler *et al.*, 1971; Nairn and Solia, 1980). *Subglacial volcanism* (Noe-Nygaard, 1940; see Chapter 13) is best known from its products, including massive floods (*jökulhlaups*), table mountains (*tuyas* or *stapi*), and ridges (*tindars* or *mobergs*). In all these environments, a major factor determining the expression of hydrovolcanism is the abundance of water available to interact with the magma. Not only are the eruptive phenomena affected by water abundance, but so are the characteristics of the interaction products, their dispersal, and the resulting landforms (Fig. 11.2).

11.2.3 Hydrovolcanic eruption styles

A wide variety of eruption styles result from magma–water interactions, ranging from passive lava effusion to highly energetic thermohydraulic explosions, depending on ambient conditions and the proportions of water and magma interacting (Fig. 11.2). At the highest

water abundances, explosive activity is generally suppressed, producing passive quenching and thermal granulation of lava flows (but see Chapter 12 for further discussion of deep-sea explosive activity). At somewhat more favorable water/magma mass ratios, surtseyan activity is a common expression of explosive hydrovolcanism in, for example, shallow marine environments. Dense, tephra-laden, cypressoid ("cock's tail") jets and steam clouds contain a significant component of liquid water, both as a result of vapor condensation and direct ejection from a shallow-water environment. Tephra is dispersed as fall or surges, which may be expressed as massive or planar-to-duneform bedded deposits. Phreatoplinian eruptions are the result of more intense interactions that produce a greater vapor-phase component at water–magma mass ratios approaching the optimum for energy conversion efficiency. Groundwater or shallow surface water is typically involved. Greater energy release allows for explosive vapor expansion, thorough magma fragmentation and the formation of convecting columns, and significantly more widespread tephra dispersal through fall and pyroclastic density currents. Duneform bedding becomes more common for energetic surge deposits. Transient explosive activity, i.e., vulcanian eruptions, may also be driven in part by pressurized vapor derived from meteoric water (Chapter 7). The deposits of phreatoplinian and vulcanian eruptions exhibit fewer indications of a liquid water phase in comparison to surtseyan deposits; the former are sometimes termed "dry" hydrovolcanic deposits, whereas the latter are termed "wet". Subglacial eruptions, discussed in detail in Chapter 13, commonly exhibit a range of hydrovolcanic styles (from pillow effusion to surtseyan and phreatoplinian activity) during their eruption sequence, and understanding of magma–ice interactions benefitted greatly from recognition of tephra and deposit characteristics first mapped in phreatomagmatic tuff cones and tuff rings.

11.2.4 Hydrovolcanic products

Hydrovolcanic solid products include tephra, blocks and bombs, explosion breccia, pillow or sheet lava, pillow breccia, and hyaloclastite. Posteruptive hydrothermal interaction with fragmental materials may produce palagonitic and zeolitic tuff, silica sinter, and travertine. Fragmental products are termed *hydroclasts* by Fisher and Schmincke (1984), instead of *pyroclasts*, a term that refers solely to the fragmental products of explosive eruptions driven by magmatic (juvenile) volatiles. Explosive hydrovolcanic products commonly contain significant abundances of lithic fragments derived from explosive fragmentation of country rock in various hydrovolcanic environments.

Petrographic studies of hydroclastic products involve the determination of particle size, shape, componentry (magmatic vs. lithic) and textural characteristics, and the chemical signatures caused by both rapid and slow alteration. These data are indicators of the degree and type of water interaction. For example, the grain size of hydroclasts is a function of the mass ratio of water and magma involved dynamically in the interaction; grain textures are indicative of the type of interaction – passive, explosive, brittle, or ductile. Field characterization of hydroclastic products focuses on analysis of deposit characteristics, including bedding, grading, sorting, lithification, and deposit thickness vs. distance from the vent. Variations of these characteristics within or among deposits can elucidate variability in eruptive intensity and style (e.g., fall vs. density current deposit), and degree of magma–water interaction.

Experimental and field research revealed a correlation between the median grain diameters of hydroclasts and the interacting water/magma mass ratio (Fig. 11.3). In general, hydrovolcanic tephra are distinguishable from magmatic tephra by their much finer grain size. Furthermore, for hydrovolcanic tephra there is an optimum water/mass ratio that produces the most thorough fragmentation; ratios less than or greater than the optimum value result in less finely fragmented tephra.

Microscopic examination of grain shapes and textures also reveals features indicative of hydrovolcanic origins; whereas the products of purely magmatic fragmentation are dominated

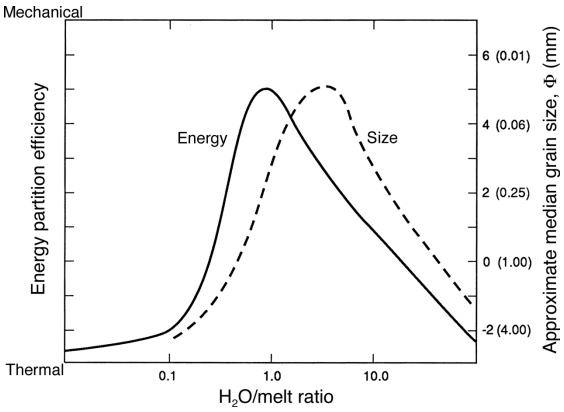

Figure 11.3 Correlation of grain size and thermal-to-mechanical energy partitioning to water/melt ratio (adapted from Frazzetta *et al.*, 1983, and Sheridan and Wohletz, 1983).

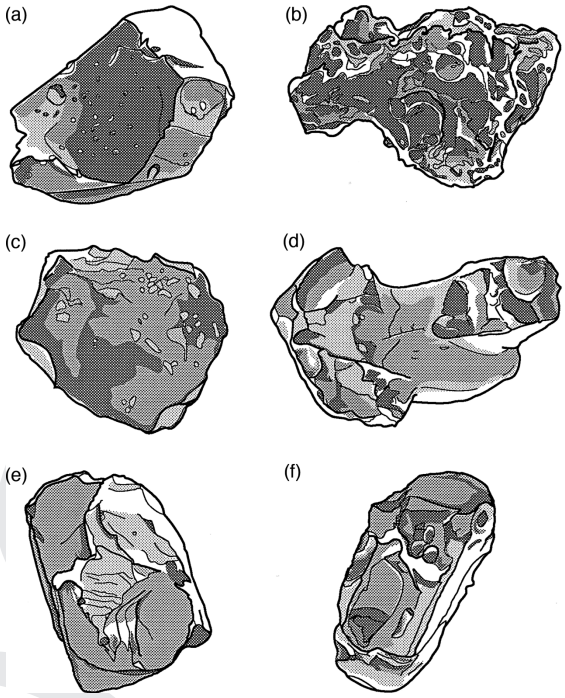

Figure 11.4 Sketches of particle textures found in hydrovolcanic deposits. (a) A characteristic blocky and equant glass shard, (b) a vesicular grain with cleaved vesicle surfaces, (c) a platy shard, (d) a drop-like or fused shard, (e) a blocky crystal with conchoidal fracture surfaces, and (f) a perfect crystal with layer of vesicular glass. In contrast, magmatically fragmented deposits are dominated by highly vesicular clasts, but may contain minor proportions of particle types shown here. (Adapted from Wohletz and Heiken, 1992.)

by highly vesicular clasts, hydroclast populations include poorly to non-vesicular clasts with a variety of textures (Fig. 11.4). Hydrovolcanic tephra may show features of both magmatic and hydrovolcanic origin; in such cases, detailed statistical study of tephra samples can help determine the relative proportions of the two end member fragmentation processes (Büttner *et al.*, 1999; Dellino *et al.*, 2001). Some hydroclastic grain textures are also indicative of the type of magma–water interaction (e.g., whether a superheated vapor or liquid phase was involved; Wohletz, 1983). For example, quench cracks on grain surfaces indicate quenching in contact with excess liquid water, and chemical pitting is indicative of contact with corrosive fluids (Wohletz, 1987; Dellino *et al.,* 2001).

Field characteristics of deposits are also indicative of the proportion of liquid vs. vapor phases in phreatomagmatic eruptions. Broadly speaking, liquid water will produce more cohesive deposits that may contain accretionary lapilli, soft-sediment deformation structures, vesiculated tuffs (due to post-depositional vaporization of liquid water), and may produce steeper landforms (e.g., tuff cones) with some degree of hydrothermal alteration (e.g., palagonitization). In contrast, more energetic eruptions producing a superheated vapor phase may result in broader, lower landform (e.g., maars, tuff rings) due to the greater mobility of the products (in falls or surges), with limited alteration of the hydroclasts. An individual eruption can evolve towards wetter or dryer conditions, which would be reflected in the deposit characteristics.

Explosive hydrovolcanic eruptions may occur as single, monogenetic events or at polygenetic centers (volcanoes constructed of multiple eruptions). The former commonly produce maars, tuff rings or tuff cones, depending on the environment of interaction and availability of water. The latter may simply introduce a phreatomagmatic deposit into the record of activity at that particular volcano.

11.3 Magma–water interaction physics

11.3.1 Fuel–coolant interactions

Formulating an understanding of the physics of magma–water interactions requires consideration of the physical properties of magma, the thermodynamic behavior of water, and the physics of processes at the interface between the two fluids. Much of the physical understanding of hydrovolcanism has developed from the combined insights derived from studies of *molten fuel–coolant interaction* (MFCI or FCI) and laboratory experiments designed to replicate hydrovolcanic phenomena (e.g., Wohletz *et al.*, 1995a; Zimanowski *et al.*, 1997a). The field of FCI science arises from industrial applications, and concerns the interaction of two fluids for which the temperature of one (fuel) is above the vaporization temperature of the other (coolant) (Buchanan and Dullforce, 1973; Buchanan, 1974). Application of FCI theory to hydrovolcanic eruptions is described in Wohletz *et al.* (1995a), Zimanowski *et al.* (1991), and Zimanowski (1998). Figure 11.5 depicts a hypothetical geologic system in which magma (fuel) explosively interacts with water-saturated sediments (coolant). The stages of a FCI are as follows:

(1) Initial contact and coarse mixing of fuel and coolant, growth of vapor film;
(2) Quasi-coherent collapse of all vapor films in the premix caused by a triggering pressure pulse (seismically induced or by local overexpansion), leading to direct contact of fuel and coolant;
(3) Cycles of enhanced fuel–coolant heat transfer, rapid (<1 ms) coolant expansion, fine fragmentation of fuel, producing superheated and pressurized water, and explosive energy release;
(4) Volumetric expansion of fuel–coolant mixture as superheated water transforms to superheated steam.

The process does not necessarily evolve through all these stages and may be arrested, for instance, before mixing or explosion.

Experimental studies have made it possible to quantify some controlling parameters by using field and laboratory measurements of hydrovolcanic products. The curves in Figure 11.3 were derived from early experiments (Wohletz, 1983; Wohletz and McQueen, 1984) that demonstrated that the explosive efficiency of the system (measured as the ratio of eruptive kinetic energy to magma thermal energy) is related to the mass ratio of interacting water and melt (thermite – a magma analog) and the confining pressure. These experiments displayed a variety of explosive and non-explosive behaviors that are analogous to natural volcanic activity, including classical strombolian, surtseyan, vulcanian, and plinian phenomena.

Experimental studies demonstrate that the thermodynamics of heat transfer (see Section 11.4.1) is a significant aspect of hydrovolcanic systems and their physical and chemical effects. The magmatic thermal energy transformed by interaction with external water is partitioned into many possible forms, including mechanical fragmentation of the magma and country rock, excavation of a crater, acceleration and dispersal of tephra, seismic and acoustic perturbations, and chemical processes such as solution and precipitation, and mass diffusion. Section 11.4.4 addresses energy partitioning further.

11.3.2 Physical properties of magma

Magma generally is treated as a three-phase system of melt, solids, and gases (see Chapter 4). The physical properties of magma are strongly controlled by chemical composition, the proportions and types of solid content (phenocrysts, xenocrysts, and xenoliths), presence of exsolved and dissolved gases, flow speed, and temperature. Natural silicate melts have temperatures that exceed the solidus by ~100–200 K, such that the heat content of magma comprises a significant proportion of latent heat. However, during rapid cooling processes relevant to many magma–water interactions, the release of latent heat is negligible, because quenching (and the formation of glass) takes place, rather than crystallization.

Magma viscosity is the result of interaction between internal friction of the melt and

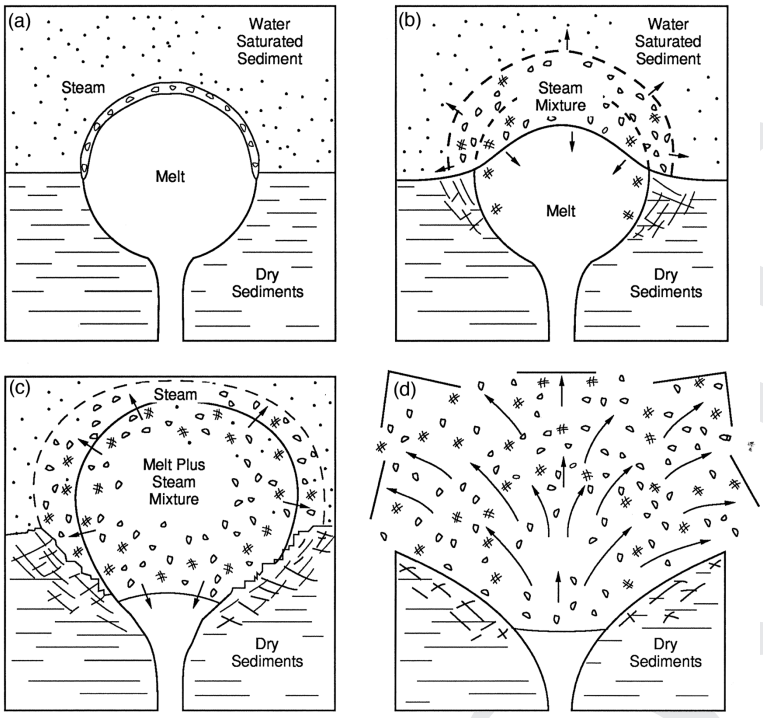

Figure 11.5 Hypothetical setting of subsurface hydrovolcanic activity, showing (a) initial contact of magma with water-saturated sediments, (b) vapor film growth, (c) mixing of magma with the sediments, and (d) expansion of the high-pressure steam in an explosion (adapted from Wohletz and Heiken, 1992).

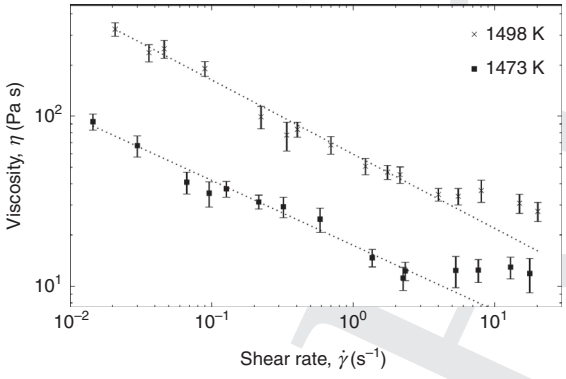

Figure 11.6 Shear stress dependent viscosity of a basaltic melt (<5 % crystals, <2 % bubbles), at two temperatures. The lines are viscosity calculations from a power-law model (modified from Sonder *et al.*, 2006).

mechanically coupled compressible bubbles and incompressible crystals (see Chapter 4, Section 4.5). Crystals are not only characterized by various morphologies, but also by various interfacial couplings (e.g., wetting angles). It is therefore not surprising that the rheology of magma needs to be addressed by a non-Newtonian model. Viscosity is not only temperature dependent, but also strongly depends on the shear rate (Fig. 11.6). At high confining pressures (i.e., at depth within the crust or beneath water), magma viscosity depends primarily on the behavior of dissolved volatiles, and will generally decrease with increasing pressure. Although this pressure-dependence is not yet well characterized, it is the viscosity contrast between magma and water that primarily governs interaction dynamics, so little effect is expected on the hydrodynamics of the magma–water system at increasing pressure.

The intensity of magma–water interactions reflects the efficiency of heat transfer at the magma–water interface, which in turn reflects the degree of magma fragmentation. Fragmentation can generally be viewed as taking place in one of two regimes, depending upon whether the characteristic deformation time is greater or less than the mechanical relaxation time of the melt: (1) *hydrodynamic* fragmentation is restricted to deformation of two-dimensional interfacial areas (boundaries between the melt and gas) and is most efficient in systems subjected to high strain rates (rapid flow) at low

viscosities, low interfacial tension, and high density contrast between the accelerating fluid and surrounding media; (2) *brittle* fragmentation is the result of three-dimensional crack growth caused by strain that exceeds the elastic properties of a medium (e.g., bulk modulus; cf. the stress and strain-rate criteria discussed in Chapter 4, Section 4.6). For hydrodynamic fragmentation to produce fine ash (< 63 μm), the required accelerations are extremely high. However, brittle fragmentation can readily produce fine ash particles through a steady increase in strain. The features of natural particles, experimental results, and theoretical models clearly show ash generation is dominated by brittle fragmentation (Zimanowski *et al.*, 2003). The material parameter that controls the brittleness of magma (i.e., the mechanical deformation energy needed to produce new crack surfaces) is the critical shear stress. The range of critical shear stress of magma is as large as the variability of viscosity, but in contrast to viscosity, the critical shear stress decreases with increasing silica content. Therefore, basaltic magma can be more than three orders of magnitude stronger than rhyolitic magma. Bubbles and crystals both weaken the structural strength and therefore reduce the critical shear stress. Further information on experimental and theoretical fragmentation studies can be found in Hermann and Roux (1990), Zimanowski *et al.* (1997a, 1997b, 2003), and Büttner *et al.* (1999, 2002, 2006).

11.3.3 Water physics

The thermodynamic behavior of water is well known from the steam-locomotion era, and many volcanological studies have approached the problem of magma–water interaction rather simplistically, by direct application of the first law of thermodynamics. While this approach does provide some limiting conditions, it ignores complex issues concerning the multi-phase (steam, water, magmatic particles, melt) system. Consideration of multi-phase fluid mechanics places further constraints on the application of thermodynamics to this problem, as described by Delaney (1982) and Wohletz (1986), and embodied in studies of MFCI (Section 11.3.1).

A crucial parameter for the behavior of water at a high temperature interface is the phase transition temperature of water into steam. In steady-state, equilibrium thermodynamic conditions, the phase transition occurs at the boiling point, which depends on the ambient pressure. However, dynamic (short duration) events require application of quasi-steady-state thermodynamic models. Instead of the phase change occurring at the boiling point and spreading outward from discrete nucleation sites, the water is heated so rapidly that it greatly overshoots its boiling temperature, reaching the homogeneous nucleation temperature (HNT), where all of the water spontaneously changes state. The boiling regime of water under atmospheric conditions starts at 373 K and the HNT is reached at ~583 K. Little is known about the pressure dependence of the HNT. During extremely rapid heat transfer, as occurs in explosive MFCI, the critical point of water (22 MPa and 647 K) may be exceeded, so that water exists as a supercritical fluid, with no phase boundary separating vapor and liquid. Experimental observations indicate that water can remain at liquid state densities even at magmatic temperatures during such interactions (Zimanowski *et al.*, 1997b).

Given that > 60% of the Earth's surface is covered by oceans, magma–water interactions predominantly involve seawater. Seawater is a solution dominated by the presence of salts (mostly NaCl), and its thermodynamic behavior can be approximated by the two-component system of pure water and NaCl. Figure 11.7(a) illustrates a p–T phase diagram for the system NaCl–H_2O that shows phase boundaries of the pure components and projections of the phase boundaries for intermediate compositions. The salinity of seawater results in critical conditions occurring not at a single point but along a curve that connects the critical points of the two pure end members. These phase relationships (Fig. 11.7(a)) show that at any temperature two fluid phases can coexist and a single critical point does not exist if solid NaCl is present. Critical behavior occurs at pressures and temperatures elevated from those of pure water to values approaching ~30 MPa and ~680 K for seawater with a salinity of 3.2 wt % NaCl (Bischoff and

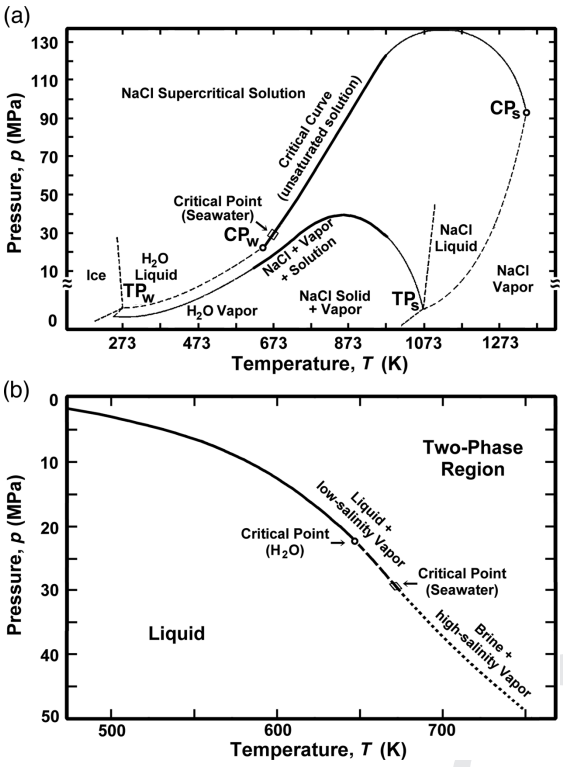

Figure 11.7 (a) Pressure–temperature diagram for the system NaCl-H_2O adapted from Krauskopf (1967) from experimental data of Sourirajan and Kennedy (1962). This diagram shows both pure H_2O and NaCl end members (dashed lines). The solid lines (bold are experimental data) schematically represent the phase boundaries connecting the pure end members. TP_w and CP_w denote the triple point and critical points of H_2O, respectively; TP_s and CP_s those points for NaCl. (b) The two-phase curve for standard seawater (3.2% NaCl) as a function of pressure and temperature, based on data from Bischoff and Rosenbauer (1984). Note that in this plot, pressure increases downward. The solid curve designates the boundary where pure water and seawater boundary are nearly coincidental. The boundary for pure water terminates at its critical point, whereas the boundary for seawater extends (dashed curve) to its respective critical point, along which it separates the stability regions of liquid and a mixture of low-salinity vapor and liquid. The phase boundary extends (dotted curve) from seawater's critical point to higher temperature and pressures, separating the liquid region from that of a mixture of high-salinity vapor and brine.

Rosenbauer, 1988). Critical pressure is expected at a depth of ~3 km in the submarine environment. Figure 11.7(a) also shows that as seawater is heated, solid NaCl is precipitated, which may greatly affect vapor nucleation (cf. White, 1996).

The two-phase boundary of seawater (Bischoff and Rosenbauer, 1984) is similar to that of pure water for subcritical conditions in pressure–temperature space (Fig. 11.7(b)), but unlike pure water, the critical point projects nearly linearly to higher pressures and temperatures (~680 K at 30 MPa to ~750 K at 50 MPa). Below the critical point the two-phase region of seawater consists of liquid and low-salinity vapor, and above the critical point it consists of brine and high-salinity vapor. These phase relationships indicate that a vapor phase can exist even at pressures above critical for seawater.

The dissolved solids in seawater also reduce the heat capacity of seawater by several percent relative to pure water. However, this effect is relatively small compared to the factor of ~2 variation in the heat capacity of pure water over the range of pressures and temperatures relevant to hydrovolcanism. For quantitative calculations, therefore, it is convenient to substitute pure water as a workable proxy for seawater because the heat capacity and phase transition of seawater appear to have offsetting effects in situations of rapid heating; however, one must bear in mind that details of heat transfer discussed in Section 11.3.4 will likely be greatly affected by the vapor nucleation and solid precipitation behavior of seawater.

The hydrodynamic properties of water, such as viscosity, heat content, expansion coefficients, do not change drastically with increasing pressure, but they do with increasing temperature. Little is known about the effect of increasing pressure on interfacial tension. However, it can be expected that this influence is small over the range of pressures reflecting submarine volcanic scenarios. The viscosity of water increases slightly with increasing pressure but strongly decreases with increasing temperature. A salt content of 3–5 % should have no significant influence on viscosity or interfacial tension.

Because magma–water interaction can result in a relatively high-pressure and high-temperature water phase, it is important to consider

the variability of water properties near critical conditions. Figure 11.8 illustrates the variation of heat capacity, viscosity, and expansion coefficients at 30 and 60 MPa, analogous to deep submarine environments at about 3000 and 6000 m depth, respectively. Note that heat capacity, viscosity, and the isobaric expansion coefficient vary rapidly in the range 600–800 K, near the critical-point temperature (647 K). This means that small changes in temperature produce large changes in properties that determine the thermodynamic and hydrodynamic behavior of water. The large thermal gradients near the magma–water contact will produce large pressure and velocity gradients, and perturbations in water movement may result in hydrodynamic instability. For example, a supercritical fluid subjected to small pressure perturbations will tend to oscillate in density (Greer and Moldover, 1981) between liquid and vapor states (e.g., growth and collapse of vapor bubbles). The speed at which water flows from higher to lower pressure regimes depends not only on the magnitude of the pressure gradient but also on the viscosity; rapid viscosity fluctuation may enhance or dampen convective currents. These pronounced fluctuations in properties are critical to address with respect to magma–water interaction. This thermal-hydraulic system has received considerable attention for application to coolant flow stability in nuclear reactors (e.g., Ruggles *et al.*, 1989, 1997).

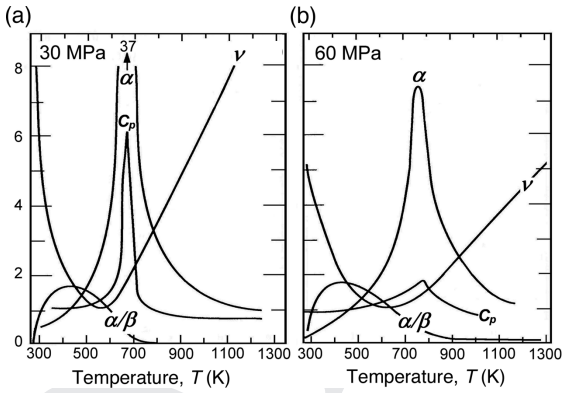

Figure 11.8 Variation of physical properties of water at (a) 30 MPa (~3000 m depth) and (b) 60 MPa (~6000 m depth) as a function of temperature. The properties are shown as curves designated by symbols and their corresponding SI units and scale factors are: α, isobaric expansion coefficient ($\times 10^3$ K^{-1}); α/β, pressure coefficient ($(dp/dt)_v$; $\times 10^{-2}$ MPa K^{-1}) where β is the isothermal expansion coefficient; ν, kinematic viscosity ($\times 10^{7-7}$ m^2 s^{-1}); and c_p, the constant pressure heat capacity (4.184 kJ kg^{-1} K^{-1}). Note the sharp inflections and discontinuities apparent near the critical temperature. (Adapted from Wohletz and Heiken, 1992.)

11.3.4 Physics of the magma–water interface

Magma provides a high temperature heat source, such that the magma–water system is somewhat analogous to the thermal coupling and heat transfer to a liquid coolant (water or aqueous liquids) used in power plant systems (e.g., Baierlein, 1999, Bejan and Eden, 1999). The major difference between magma–water interactions and power plant heat flow problems is that the interface conditions in a boiler are of a fixed geometry, whereas the magma–water interface is always dynamic. The heat flux from the magma–water interface to the water greatly exceeds the heat flux from the magma to the interface because of the relatively low magma thermal conductivity (~1 W m^{-1} K^{-1}; Büttner *et al.*, 1998, 2000, Ebert *et al.*, 2003), and limited convection due to its high viscosity. Consequently, the temperature at the hot side of the interface drops rapidly, leading to solidification of the magma. Because the thermal conductivity of quenched melt is more than twice that of its liquid state, a cooling front migrates into the magma. Once a certain thickness has solidified, the strain caused by the 1–3% decrease in volume at the glass transition temperature leads to the formation of cooling cracks (thermal granulation) and thus to fragmentation of the magma into relatively coarse particles. This process has the potential to greatly increase the interfacial area between magma and water. The balance between quenching and surface area growth rates determines whether the heat transfer is relatively steady, or whether the heat transfer rate escalates. Section 11.4.1 discusses the thermodynamic regimes within which the heat transfer takes place. It is not only thermally induced fragmentation that modifies the heat flux, but also external hydro-mechanical

forcing, such as differential movement between magma and water, and seismic impulses (earthquakes), which can affect the stability of the magma–water interface. Experimental studies suggest that external triggering is a major mechanism leading to the escalation of heat transfer into explosive conditions. For more details on magma–water mingling/mixing and fragmentation physics see Morrissey *et al.* (2000) and Zimanowski and Büttner (2002, 2003).

In contrast to the hydrodynamics discussed in Section 11.3.3, the thermodynamic behavior of the magma–water interface changes dramatically with increasing temperature and hydrostatic pressure, and the effects of mineralization (e.g., seawater) are generally small by comparison. The thermal coupling between magma and water is largely dependent upon the interface temperature and development of a vapor film between the magma and the water. The vapor film consists of two regions: (1) a thicker hot layer of superheated steam at the same temperature as and directly in contact with the magma, and (2) a thinner cool layer (the *thermal boundary layer*) between the superheated steam layer and water, within which condensation and vaporization balance. The temperature of the thermal boundary layer can be only microscopically defined because its thickness may be much less than a few millimeters. Because the interface temperature is a hypothetical value, dependent upon thermal diffusivities of magma and vapor, it is useful to characterize the vapor-film by its temperature contrast with the magma (i.e., the magma surface temperature minus water temperature). In so doing, the transfer of heat energy between substances, known as *thermal coupling*, can be classified in three regimes, with coupling increasing from (1) to (3):

(1) *Stable-film boiling*: At a temperature contrast well above the water HNT and an ambient pressure well below the critical pressure of water, a macroscopic vapor film forms at the interface between magma and water and restricts the thermal coupling. The thickness of the vapor film is greater for high temperature contrasts and low ambient pressures.

(2) *Metastable-film boiling*: At a temperature contrast below the HNT, a macroscopic vapor film does not form; however, the thermal coupling is modified by local formation of steam at the interface. At a temperature contrast well above the HNT, metastable-film boiling can take place in two cases. In Case 1, high ambient pressure causes a reduction of the thickness of the superheated steam layer of the film so that it reaches the same thickness range as the thermal boundary layer. In Case 2, hydrodynamic disturbances cause interfacial instability waves with amplitudes of the same scale as the total film thickness.

(3) *Direct contact*: At a temperature contrast below the boiling point of water and/or at ambient pressures exceeding the critical point of water, the thermal coupling can be described using equilibrium thermodynamics, and it depends on the thermal properties of the liquids and the hydrodynamics at the interface. The thermal properties of magma are not strongly affected by increasing ambient pressure, however, the properties of water change markedly (Fig. 11.8). For magma and water in direct contact, the thermal coupling is one to two orders of magnitude higher than that of stable and metastable film boiling.

Considering the effect of increasing hydrostatic pressure on the thermal coupling of magma and water, the stable-film boiling regime is restricted to ambient pressures below about 1 MPa where the vapor film thickness at the magmatic temperatures of the hot layer becomes critical. Above ambient pressures of 10 MPa, the moderating effect of metastable-film boiling can practically be excluded. At thermal power plants, where an optimum heat flux (i.e., direct contact) is required, the water pressure of the heat exchange system usually is set to 15–20 MPa for temperature contrasts comparable to magmatic conditions. The thermal coupling at a constant magma–water interface at water depths exceeding ~1 km (equivalent to 10 MPa) can therefore be described well by the direct contact regime.

Magma fragmentation is an important aspect of the interface physics. Wohletz (1983)

discusses a number of hydrovolcanic fragmentation mechanisms that create a complex interface geometry, but the actual fragmentation mechanisms involved are generally categorized as hydrodynamic (ductile) and brittle (Section 11.3.2). With increasing fragmentation, the interfacial surface area increases exponentially. This increase in surface area is often referred to as mixing. The resulting mixture evolves from a pre-expanded combination of magma fragments and high-pressure water and vapor to a post-expanded mixture of quenched fragments and steam, which typically forms an eruption column. Although Kokelaar (1986) distinguishes *contact-surface interaction* (dynamics along an interface between a free body of water and magma) from *bulk interaction* (dynamics of a volume of magma that confines water or water-rich clastic materials), both cases involve heat transfer along the interface between magma and water. Experimental evidence indicates that most of the fragmentation occurs during development of interface dynamics and prior to expansion and eruption. Nevertheless, Mastin (2007) develops a strong argument for the occurrence of *turbulent shedding* of glassy rinds from fragments in erupted jets of steam and ash. The physics of the dynamic interface are complex and poorly understood; however, experimental studies of shock waves associated with interface dynamics suggest the physics may involve detonation, i.e., the formation of an exothermic shock front whose propagation creates an explosion.

Wohletz (2003) discusses how film boiling can be intimately linked to fragmentation and interface surface area increase. The interface becomes not only thermodynamically unstable with metastable film boiling, it is also hydrodynamically unstable because of large pressure, density, sound speed, and conductivity gradients produced by the film. Such instability is prone to a kind of detonation, termed *thermal detonation*, especially if perturbed by some external pressure wave, such as that produced by volcanic seismicity. In a thermal detonation, the acceleration of the particle mixture by the shock wave must produce a relative velocity, u_r, high enough to satisfy the Chapman–Jouguet (C–J) condition: u_r is the speed of the shocked material relative to the shock front, and u_r must equal the sonic velocity of the shocked material (Courant and Friedrichs, 1948; and Zel'dovich and Raizer, 1966).

The C–J condition can be evaluated on a pressure–volume diagram (Fig. 11.9) that shows the shock adiabat (termed the *Hugoniot* and defined as the locus of points representing pressure–volume states achievable by shocking a material from an initial state) and the release adiabat (called the *Rankine–Hugoniot curve* or *detonation adiabatic*). These adiabats are concave upward and the detonation adiabatic exists at higher volume states than the Hugoniot. The detonation adiabatic is defined by classical Rankine–Hugoniot jump conditions for conserving mass, momentum, and energy across a shock wave (Landau and Lifshitz, 1959; Zel'dovich and Kompaneets, 1960; and Zel'dovich and Raizer, 1966). These conditions can be stated as:

$$\rho_1 u_1 = \rho_2 u_2; \quad \text{(mass)} \tag{11.1}$$

$$p_1 + \rho_1 u_1^2 = p_2 + \rho_2 u_2^2; \quad \text{(momentum)} \tag{11.2}$$

$$E_2 - E_1 = \frac{1}{2}(p_1 + p_2)(V_1 - V_2); \quad \text{(energy)} \tag{11.3}$$

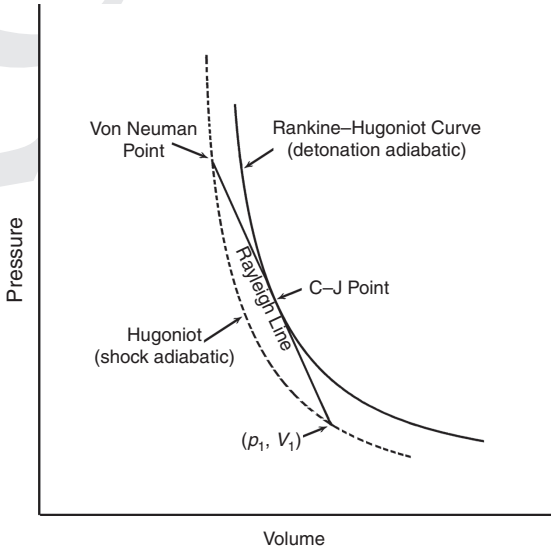

Figure 11.9 Pressure–volume diagram showing the relationships among the initial state of the magma–water mixture (p_1, V_1), the shock Hugoniot, the Rayleigh line, the Von Neumann and Chapman–Jouguet (C-J) points, and the detonation adiabatic.

where ρ is mixture density, V is mixture specific volume = $1/\rho$, p is pressure, u is mixture velocity, $E = E(p,V)$ is mixture internal energy, and subscripts 1 and 2 indicate the unshocked and shocked states. All notation is given in Section 11.6. For an inert material, the shocked thermodynamic states given by Eq. (11.3) define the Hugoniot, which is typically determined experimentally to derive the equation of state of a material. Two points on the Hugoniot, one at the initial pressure (p_1,V_1 in Fig. 11.9) and the other at the pressure of the shock front (the *von Neumann point* or *spike*, since there is a transient pressure peak at this location), define the *Rayleigh line*. For a reactive material in which the shock induces vapor production in its wake (either chemically for common explosives, or physically for a magma–water mixture where nearly instantaneous heat transfer produces vapor), the energy equation (Eq. 11.3) gives all possible states of the detonation adiabatic (Fig. 11.9).

By combining Eqs. (11.1) and (11.2), one obtains the value of $(p_2 - p_1)/(V_1 - V_2)$, which is a constant defined by the slope of the Rayleigh line. The square root of this slope is proportional to the velocity of the detonation wave. Zel'dovich and Kompaneets (1960) show that the only possible steady state (in which a detonation wave is sustained) is where the Rayleigh line is a tangent to the detonation adiabat at the C–J point. The points behind a propagating shock at which the C–J condition exists define a surface known as the *C–J plane* or the *detonation front* (not to be confused with the shock front).

Figure 11.10 shows a generalized conceptual view of thermal detonation that includes observed phenomena such as thermohydraulic fracturing and brittle reaction, described by Zimanowski *et al.* (1997b) and Büttner and Zimanowski (1998), which lead to enhanced heat transfer and catastrophic vapor expansion. Zimanowski *et al.* (1997a) document experiments that show development of intense shock waves in less than a millisecond under extreme rates of cooling ($> 10^6$ K s^{-1}) and stress (> 3 GPa m^{-2}). Yuen and Theofanous (1994) demonstrate that application of detonation theory successfully predicts results of many of their MFCI experiments. In order to assess the role of ambient pressure in hydrovolcanism using detonation theory, the method of Board *et al.* (1975) can be used to calculate (using the Rankine–Hugoniot jump conditions) the speed of a propagating shock wave through a magma–water mixture. For mixture conditions of $R \sim 0.5$ (where R is the mass ratio of water to magma), a shock speed is ~300 m s^{-1}. This velocity defines a Rayleigh line slope, and then the Rankine-Hugoniot conditions must be specified in order to predict a detonation adiabatic that touches the Rayleigh line at a single point of tangency, the C–J condition of (p_{cj}, V_{cj}). To induce mechanisms for melt breakup (Fig. 11.10), the C-J condition requires that the slip velocity u_s between the shocked melt fragments and water is at least as large as u_r. Using the classical detonation theory described by Eqs. (11.1)–(11.3), the relative velocity of the shocked mixture leaving the front is a function of the mixture pressure and specific volume at initial and C–J conditions:

$$u_r = \sqrt{(p_{cj} - p_1)(V_1 - V_{cj})}. \tag{11.4}$$

For an idealized thermal detonation in which $p_{cj} \approx 100$ MPa (Board *et al.*, 1975), Eq. (11.4) sets u_r at ~100 m s^{-1}. For volcanic MFCIs, the approach of Corradini (1981) yields a minimum u_r of 60 m s^{-1} (Wohletz, 1986). Drumheller (1979) combined the requirements for relative velocity and melt breakup time into a *critical Bond number* (the Bond number is ratio of body and surface tension forces). By assuming a constant p_{cj}, Wohletz (1986) evaluated the critical Bond number with respect to MFCI experimental data (Wohletz and McQueen, 1984) to predict the effects of R and ambient pressure on the development of relative velocities and magma particle sizes. Optimal conditions for thermal detonation exist at $0.5 < R < 2.0$, for ambient pressures ≤ 40 MPa (Wohletz, 2003). With increasing ambient pressure, predicted relative velocities fall to < 60 m s^{-1} (which is considered the lower limit for sustaining a detonation; Wohletz, 1986), and particle fragmentation decreases, meaning less thermal energy is released in the wake of the shock wave.

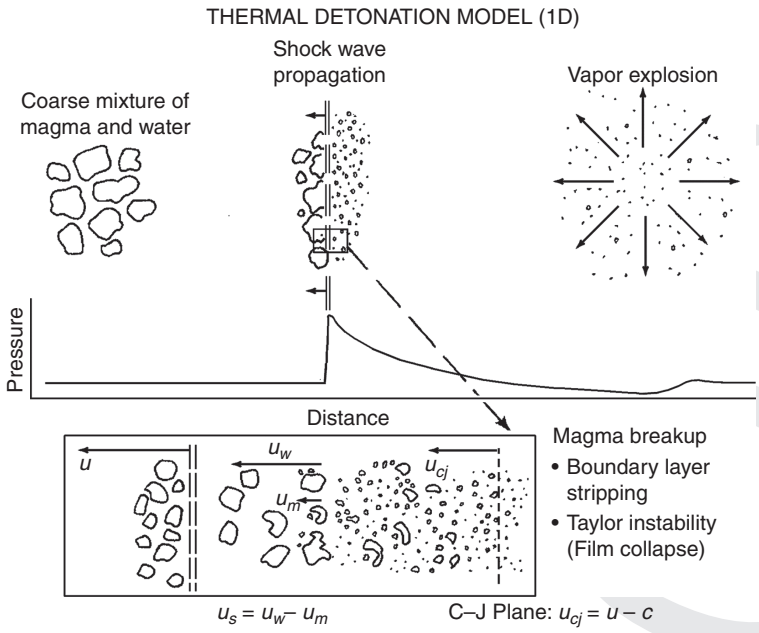

Figure 11.10 Schematic illustration of thermal detonation (adapted from Wohletz, 2003; Board *et al.*, 1975), showing propagation of a shock wave through a coarse mixture of magma fragments and water (vapor and liquid). The shock wave moves at velocity u and differentially accelerates the water and magma to velocities of u_w and u_m, respectively, resulting in a slip velocity u_s, which decays behind the shock. The slip velocity must be of sufficient magnitude to cause fine fragmentation of the magma fragments by mechanisms that shear away the boundary layer and cause interpenetration of the water and magma (Taylor instability) before the arrival of the C–J plane. At the C–J plane, the average mixture velocity is just sonic with respect to the shock wave. Fine fragmentation causes an exponential rise in heat transfer from the magma fragments to the water (characteristic conductive heat transfer times are ~ tens of μs for fine fragmentation) and catastrophic vapor expansion.

11.4 Modeling magma–water interaction

11.4.1 Experimental insights into magma–water interaction

Experimental research on magma–water interaction has been strongly influenced by FCI studies in the context of nuclear safety research (e.g., Board *et al.*, 1975; Corradini, 1981; Henry and Fauske, 1981; Theofanous, 1995). Since the early 1980s, laboratory experiments have been conducted on magma–water interaction (e.g., Wohletz *et al.*, 1995a; Zimanowski *et al.*, 1997a; Büttner and Zimanowski, 1998), in which high-temperature melt (predominantly remelted volcanic rocks at ~1270 K) is brought into contact with water (Fig. 11.11). The philosophy of the experiments was to achieve a mesoscale dimension, minimizing danger, costs, and experimental effort, while fully representing the relevant physics. As discussed in Section 11.2.4, important information on natural explosive magma–water interaction is found in the characteristics of the products (tephra). In the experiments, the physical processes can be observed and

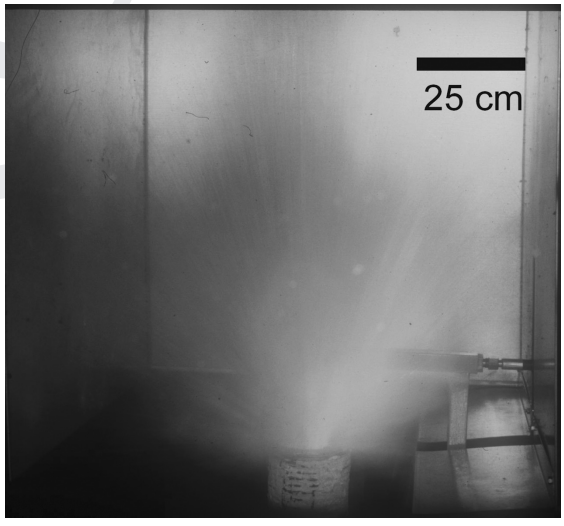

Figure 11.11 Explosive interaction after injection of water into molten basaltic rock (Physikalisch-Vulkanologisches Labor, Universität Würzburg). See color plates section.

Figure 11.12 Products of thermal granulation experiments using remelted basalt (Physikalisch-Vulkanologisches Labor, Universität Würzburg).

measured directly. To verify the relevance to natural volcanic processes, the experiments were designed to produce artificial tephra in statistically relevant quantities. Furthermore, the products were nearly identical to the natural analogs in terms of grain-size, morphology, and chemical composition (Fig. 11.12).

Experimental results demonstrate that the intensity of magma–water interaction, and thus the danger potential of hydrovolcanic eruptions, depends on the efficacy of the heat transfer from magma to water, i.e., the amount of heat transferred per unit volume and time. As discussed in Section 11.3.4, this heat transfer is directly correlated to the interfacial area (i.e., the size of the contact area between magma and water per unit volume) and the interfacial coupling conditions. Heat transport in the magma to the interface is controlled by the temperature-dependent magma thermal conductivity; convection can be neglected because of the high viscosity of magma and the short timescale. Heat transport in the water (having a viscosity at least three orders of magnitude less than magma) away from the interface is controlled by both conduction and convection, and therefore is in principle much more effective. The thermal coupling at the interface can be described in the three regimes: of stable film boiling, metastable film boiling, and direct contact, with direct contact producing about two orders of magnitude greater heat flux per unit area than stable film boiling (Section 11.3.4). Three heat flux regimes in the magma–water system can be defined to allow classification of magma–water interaction and facilitate theoretical description of the thermodynamics and hydrodynamics of the system (Wohletz, 1995; Büttner and Zimanowski, 1998; Zimanowski *et al.*, 2003; Büttner *et al.*, 2005):

(1) *Non-explosive interaction regime.* The heat flux in the system does not create a water overpressure (subcritical state of coolant). Steady thermodynamic sink conditions are maintained (i.e., water can always be described as a passive heat sink and steady-state thermodynamic models are applicable). Fragmentation of magma is governed by its rheology in an aqueous environment (e.g., pillow formation) and/or by thermal contraction of melt (thermal granulation), leading to passive fragmentation (Schmid *et al.*, 2010; Sonder *et al.*, 2011).
(2) *Subsonic explosive interaction regime.* The heat flux in the system creates a water overpressure (critical state of coolant). Superheated water is generated and complex phase transitions occur. Steady-state thermodynamic models need significant modifications, but still are generally applicable. Fragmentation

(of magma is dominated by brittle processes caused by the hydraulic forcing of the coolant, but governed by the mechanical properties of the magma (i.e., mechanical deformation does not exceed critical shear conditions and propagation of cracks is subsonic with respect to the shear-wave velocity). This regime leads to subsonic active fragmentationAustin-Erickson *et al.*, 2008).

(3) *Supersonic explosive interaction regime.* The heat flux in the system increases rapidly, due to a thermohydraulic feedback mechanism and high overpressure is generated in the water (supercritical state of coolant). Non-equilibrium thermodynamic models are recommended. Fragmentation of magma is driven by hydraulic forcing of the coolant exceeding the mechanical properties and propagation of cracks is supersonic. Consequently a significant proportion (up to 80%) of the mechanical energy is released as shock waves. This regime leads to supersonic active fragmentation.

The consequences for the eruptive behavior of the magma–water system depend on the interacting magma/coolant volume ratio, the rheological properties of the magma, the thermal and rheological properties of the coolant, the hydrodynamic mingling energy, the ambient pressure, and the geometry of the mingling space. In the following section, we discuss modeling techniques for steady state regimes 1 and 2 and the non-equilibrium conditions of regime 3.

11.4.2 Multiphase equilibrium thermodynamic models

Simple conservation of energy provides for a first-order assessment of magma–water interactions. For most cases, the magma temperature exceeds the water vaporization temperature, which varies somewhat with composition and ambient pressure. During interaction, the internal energy of the water increases by an amount equal to that lost by the magma. While most of that internal energy is involved in heating the water and quenching the magma, some of it may also be involved in phase transitions (e.g., water vaporization and magma crystallization). During explosive interaction the energy exchange happens rapidly, resulting in a minimum of energy going towards phase transitions and most going towards raising the temperature of the water and cooling the magma. For this simple situation, the equilibrium temperature, T_e, is between the temperature of the magma, T_m, and that of the water, T_w. Therefore, simple energy conservation can be expressed as:

$$m_w c_w (T_e - T_w) = m_m c_m (T_m - T_e), \tag{11.5}$$

where m is the mass and c is the specific heat capacity of the water (subscript w) and the magma (subscript m), respectively. Equation (11.5) shows that T_e varies with the mass ratio of water to magma, m_w/m_m, denoted as R. In addition, the specific heat ratio of water to magma is typically in the range of 3.0 to 4.0, depending upon magma composition and the range of typical water states at the surface of the Earth. For most cases, it is assumed that the ratio $\xi = c_w/c_m \sim 3.5$. Accordingly, we can rearrange Eq. (11.5) to predict T_e:

$$T_e = \frac{\xi R T_w + T_m}{1 + \xi R}. \tag{11.6}$$

The value of T_e can be thought of as an idealized initial thermal equilibrium prior to explosive vaporization of the water, which allows thermodynamic prediction of the resulting mechanical energy of the interaction. Figure 11.13(a) shows some predictions of T_e as a function of R. However, this thermal equilibrium is just an idealization and many factors can cause initial interaction temperatures to be higher or lower, one of which is the composition of the water.

Water at the surface of the Earth may contain dissolved or suspended constituents (e.g., muddy water), or it may be contained within pores of rock or sediments. The effect on the thermal equilibrium can be evaluated as follows. For interactions between magma and saturated rocks or impure water (White, 1996), rock and impurities act as heat sinks, and the mass ratio, R_r, is given as

$$R_r = \frac{m_r}{m_m}, \tag{11.7}$$

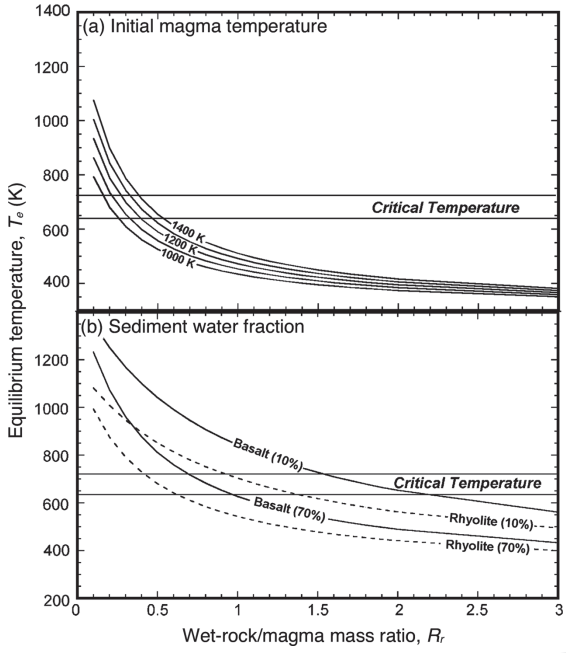

Figure 11.13 Thermal equilibrium (T_e) is the idealized temperature that water (in saturated rock) can reach during interaction with magma, and it is shown as a function of R_r (mass ratio of wet-rock/magma). These plots show cases where the initial water temperature water is 298 K and the magma heat capacity c_m is ~ 1 kJ kg^{-1}. The range in critical temperature reflects the effect of dissolved solids. (a) T_e is shown for different initial temperatures of magma interacting with water (100% volume fraction, where $R_r = R$). (b) For basalt (solid curve; 1473 K) and rhyolite (dashed curve; 1173 K) interacting with wet rocks, T_e is shown as a function of rock water volume fraction, for which 10 and 70% bound a range centered on 40% ($x_w \approx 0.2$; Eq. (11.9)), representing a porous, fully saturated sandstone.

where m_r is the mass of rock and pore water (or water plus impurities). In these situations, the water/magma mass ratio is

$$R = x_w \quad R_r = x_w \frac{\rho_r V_r}{\rho_m V_m}, \tag{11.8}$$

where x_w is the water mass fraction in a rock (or impure water) volume V_r having bulk density ρ_r, interacting with a magma volume V_m having density ρ_m. For magma interacting with pure water alone, $x_w = 1$, $\rho_r = \rho_w$, and $V_r = V_w$. In order to cast this relationship into terms of rock porosity and saturation, which are commonly measured quantities, we write the following equation:

$$x_w = \frac{S_w \, \phi \, \rho_w}{\rho_r}, \tag{11.9}$$

where S_w is the rock saturation (the volume fraction of pores filled by water), and ϕ is the rock porosity. For impure water with suspended rock particles one can consider S_w = 1 and ϕ somewhat less than unity (depending on the volume fractions of water and particles). From Eqs. (11.8) and (11.9), R may be approximated as:

$$R \approx S_w \phi \left(\frac{\rho_w}{\rho_m}\right)\left(\frac{V_r}{V_m}\right), \tag{11.10}$$

such that R can be constrained by measuring the volume ratio of lithic constituents and magma in samples of tephra or consolidated sediments such as peperite (a sedimentary rock containing igneous fragments formed during contact of magma and wet sediments).

Besides the effect on the value of R, one must also consider the heat capacity of water impurities or the porous rock containing the water. In Eq. (11.6), the heat capacity ratio ξ is replaced by the ratio involving wet rock instead of pure water, c_r/c_m. Here c_r is the effective heat capacity of the impure water or water–rock mixture, which can be approximated as a function of x_w by:

$$c_r = x_w \quad c_w + \left(1 - x_w\right) \quad c_s, \tag{11.11}$$

where c_s denotes the heat capacity of the solid constituents, and $c_s \approx c_w / 4$.

For a typical magma in contact with water-saturated rock at 298 K, T_e decreases with R_r, as shown in Figure 11.13(b). It is evident that, for magma interacting with wet rocks, T_e can exceed critical temperature (647 K (pure) to 720 K (5 wt.% dissolved solids)) where $R_r < 1.0$ (basalt) and $R_r < 0.5$ (rhyolite). Where critical temperature is exceeded during interaction prior to explosive expansion, supercritical pressures will be created.

Thermal equilibrium is probably never reached during the time span of interaction because of the insulating property of the vapor film that forms at the magma–wet-rock interface. Because of its relatively low thermal conductivity, a vapor film can greatly decrease the rate of heat transfer from the magma to the wet

rock, allowing gradual quenching. With gradual quenching, the film slowly heats water in the rocks near the magma at a rate balanced by the heat transfer away from it by the convective movement of pore water, provided that pores are interconnected. However, such passive quenching is not always the case. Consider the hypothetical instantaneous interface temperature, T_I, attained by the initial contact of magma with water that can be estimated (Cronenburg, 1980) by:

$$T_I = \frac{T_m\left(k_m/\sqrt{\kappa}_m\right) + T_w\left(k_w/\sqrt{\kappa}_w\right)}{\left(k_m/\sqrt{\kappa}_m\right) + \left(k_w/\sqrt{\kappa}_w\right)}, \qquad (11.12)$$

where k and κ are thermal conductivity and diffusivity, respectively, and subscripts m and w refer to magma and water, respectively. For the contact of a typical basalt magma with pure water, T_I approaches 1000 K. Because of the rapidity of heat exchange, water may exist in the metastable state of superheating in which it is a liquid well above its vaporization temperature. A consequence of this superheated state is that it continues to absorb heat at a high rate, reaching temperatures well in excess of its spontaneous nucleation temperature (i.e., HNT ~583 K). As temperatures approach the critical temperature (647 K), instantaneous vaporization by homogeneous nucleation produces a vapor film that expands rapidly and is highly unstable – that is, it can expand well beyond the thermodynamic equilibrium thickness. In so doing, the vapor becomes supercooled, leading to spontaneous condensation. The condensation then leads to a rapid collapse such that liquid water impacts the magma surface with a finite amount of kinetic energy, leading to a second spontaneous vaporization event. This cyclic vapor film growth and collapse is repeated continuously, typically with a frequency of up to 1 kHz (analogous to the *Leidenfrost* phenomenon of a drop of water vibrating on a hot metal surface). Vapor film instability can generate enough kinetic energy to distort the interface between the magma and wet rock, as well as cause failure of the host rock. In some cases, film collapse can lead to jets of water-saturated rock fragments penetrating the magma surface (White, 1996). In addition, the rapid heat loss from the magma by this continued vapor-film instability leads to magma quenching and possible granulation. With these interface phenomena, the magma becomes increasingly fragmented, leading to larger surface areas for heat transfer and larger volumes of superheated water and vapor.

Further thermodynamic predictions about magma–water interactions can be derived from analysis of the thermodynamic work done by the expansion of water from its initial thermal equilibrium. We have assumed that nothing is known about the mechanism of the contact between magma and water, but that it results in production of high-temperature and high-pressure water that may explosively decompress. Thermodynamic work is manifested in the fracture and excavation of country rock to form a crater, fragmentation of the magma into fine-grained debris, and ejection of these fragments in an expanding jet of steam. For a hydrovolcanic eruption, it is necessary to find the work potential for expansion of the steam to atmospheric pressure. Calculation of the true potential requires determination of a complex set of boundary conditions unique to each eruption, but for simplicity and generality, one can make some standard assumptions that allow analytical calculation of maximum potential. For the system consisting of a mixture of magmatic particles and water and the surroundings being the volcano vent structure and the atmosphere, we assume that:

(1) All heat lost by the magma during the eruption is transferred to external water;
(2) Liquid water and magma are incompressible, so that for each the specific heats remain constant with changing pressure and volume;
(3) The specific volume (reciprocal of density) of liquid water is small compared to that of its vapor;
(4) Water vapor behaves as a perfect gas and the magma volume does not change during the eruption (i.e., it does not vesiculate or contract during cooling).

Some heat is lost from the magma to both the country rock and the atmosphere during eruption, and magma does exhibit a finite volume

change on quenching. The combined effect of these caveats may account for energy discrepancies of several percent. The other assumptions concern the exact thermodynamic properties of water. At supercritical states a deviation from ideality of ≥ 10% is expected, but since most volume change occurs at subcritical states for adiabatic expansion, the assumptions introduce very little error into calculations, especially when extended or extrapolated steam table data are considered, such as by using a modified Redlich–Kwong equation of state (Burnham *et al.*, 1969; Holloway, 1977; Kieffer and Delany, 1979).

Online Supplement 11A (see end of chapter) provides a derivation of the thermodynamic work of the interaction. From this analysis, the following predictions can be made for magma interacting with water or water-saturated rock. The conversion ratio of a magma–water interaction is the fraction of magmatic heat converted to thermodynamic work, and is a measure of the mechanical energy released by the interaction. Figure 11.14(a) shows conversion ratios as a function of the wet-rock/magma mass ratio R_r for the interaction of a basaltic magma with saturated rocks (with 40% porosity and x_w = 0.2). Also shown are curves depicting pure water–magma interaction (i.e., x_w = 1). Both *isentropic* expansion (in which steam separates from fragmented magma) and *pseudo-isothermal* expansion (in which steam and fragments remain at the same temperature, denoted in figures as *isothermal*) are calculated. Note that, compared to pure water–magma interactions, wet-rock–magma interactions have lower conversion ratios (are less energetic) with optimum conversion ratios near R_r = 1.0. Figure 11.14(b) shows the fraction of vaporized water that condenses back to liquid during expansion. For interactions at low R_r values, most of the water remains in the vapor state after expansion, leading to the likelihood of explosive behavior. In contrast, for R_r > 3.0 (wet rock), a dominant portion of the steam condenses during expansion, producing a liquid–particle system. This latter behavior allows convective heat transfer that promotes passive cooling, which is less likely to be explosive.

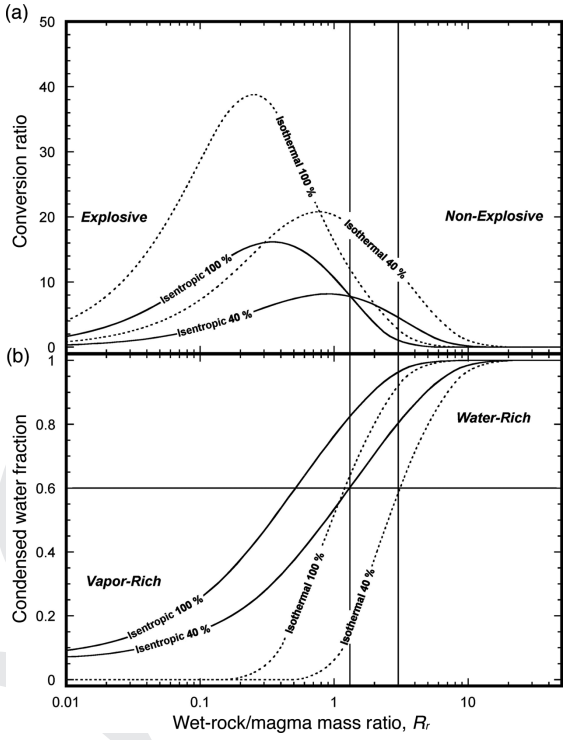

Figure 11.14 (a) Conversion ratio and (b) condensed water fraction vs. wet-rock/magma mass ratio, R_r. Solid curves are isentropic values and dashed curves are pseudo-isothermal values (labeled *isothermal*). Conversion ratio is the percentage of the magma's heat energy that is converted to thermodynamic work during interaction with water. This plot shows results for a basaltic magma at 1473 K interacting with water at 298 K (solid curves, 100% water by volume; x_w = 1) compared with those for water-saturated sediments (dashed curves; 40% porosity, 100% saturated; $x_w \approx 0.2$; Eq. (11.9)). The condensed water fraction represents the fraction of interacting water that condenses to a liquid state after expansion. For water-saturated sediment interactions having R_r > 1.3 (isentropic) to 3 (pseudo-isothermal), a dominant fraction (> 0.6) of vaporized water will condense to liquid during expansion to ambient pressures, and wet sediments have the ability to convectively carry heat from the magma, behaving as fluid substances rather than explosive vapor-rich ones. Using this criterion, an arbitrary region, separating explosive from non-explosive behavior, may be drawn over the range $1.3 \leq R_r \leq 3.0$.

Wet-rock–magma interaction may also occur at depths below the Earth's surface in hydrothermal systems of elevated temperature and pressure. Figure 11.15(a) shows that when pore water is at elevated temperatures (e.g., 358 K), a

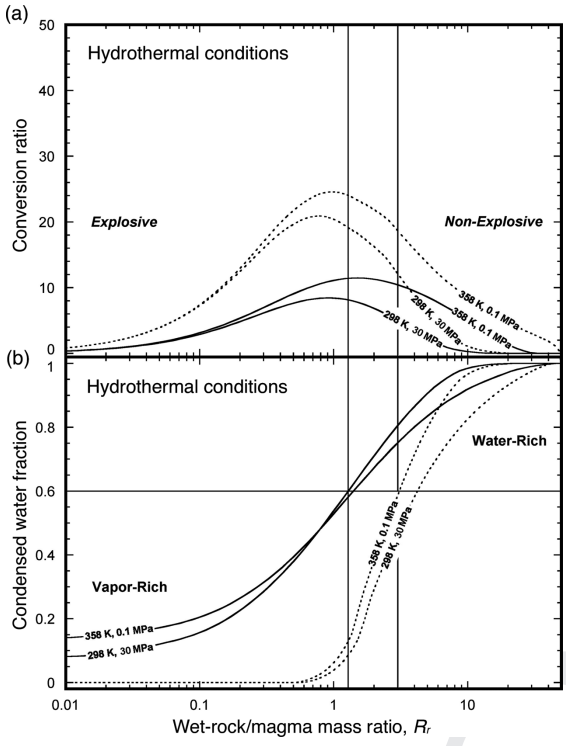

Figure 11.15 (a) Conversion ratio and (b) condensed water fraction vs. wet-rock/magma mass ratio R_r for hydrothermal conditions of elevated pore-water temperature (358 K) and elevated hydrostatic pressure (30 MPa). These curves represent a saturated sediment containing 40% by volume water ($x_w \approx 0.2$); solid curves are for isentropic expansion and dashed curves are for isothermal expansion.

slightly greater fraction of the magma's thermal energy is converted to thermodynamic work and optimum peaks occur at slightly higher values of R_r when compared to values shown in Figure 11.14(a). However, elevated hydrostatic pressure (e.g., 30 MPa) does not have much effect. Still, conversion ratios at hydrostatic pressures exceeding critical pressure are sufficiently large that such interactions could be explosive.

To further illustrate these calculations, Figure 11.16 depicts water phase diagrams with pressure-temperature-volume-entropy (*p-T-V-S*) relationships for theoretical initial equilibrium and final states. Both isentropic (Fig. 11.16(a)) and pseudo-isothermal (Figs. 11.16(b,c)) paths are shown. Isentropic expansion follows paths of constant entropy (Fig. 11.16(a)), whereas, the pseudo-isothermal expansion of the vapor–fragment mixture follows paths intermediate to those of isentropic and pure isothermal expansions (Kieffer and Delany, 1979). The phase diagrams also illustrate the three regimes of heat flux described in Section 11.4.1. The non-explosive interaction regime generally corresponds to interaction ratios $R_r > 10.0$, for which isentropic expansion is simply a vertical path in Figure 11.16(b) and water expansion is always subcritical. The subsonic explosive interaction regime approximately corresponds to interactions where $1.0 < R_r < 10.0$. For adiabatic and pseudo-isothermal expansions in this regime, water is converted to steam at high pressure but then some of it condenses during expansion. The supersonic explosive interaction regime ($R_r < 1.0$) involves significant expansion in supercritical states, especially for pseudo-isothermal conditions. The supercritical state is considered further in Section 11.4.3. It is important to note that the correspondence of these heat-flux regimes to the range of water/magma mass ratios and modeled thermodynamic states is very approximate because other factors contribute to determining the actual heat-flux regime, namely the rheology of the magma, and conditions of contact and subsequent mixing and fragmentation.

Figure 11.16 also illustrates an important point that experimental studies confirm: the critical point of water is not necessarily a limiting factor in vapor explosions. It has been commonly assumed that interactions occurring at confining pressures above the critical point of water (22 MPa) cannot result in explosions, because water exists as a supercritical fluid for which there is no liquid–vapor phase boundary. Considering the thermodynamic paths illustrated in Figure 11.16(c), where interactions are nearly an order of magnitude in excess of critical pressure, release of the interaction pressure involves a large volume increase, especially for pseudo-isothermal expansion, at rates determined by local sound speeds (Kieffer and Delany, 1979). Although the interactions extend to pressures exceeding critical, it is not yet clear if explosive expansion can initiate at these high pressures (equivalent to

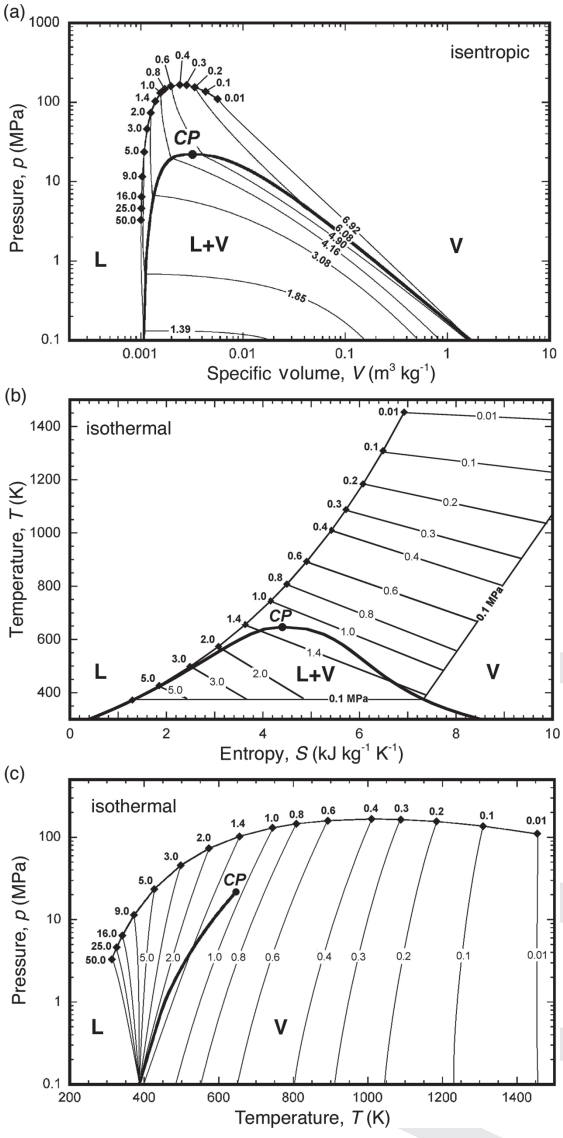

Figure 11.16 Phase diagrams illustrating calculations of wet-rock–magma interaction, using the method of Wohletz (1986). Labeled points (diamonds) are the theoretical initial equilibrium condition for interactions of various R_r (from 0.01 to 50.0; $x_w \approx 0.2$). The critical point (CP), liquid (L), vapor (V), and liquid plus vapor two-phase (L+V) regions are shown. (a) A *p*–*V* diagram shows expansion volumes and release isentropes (kJ kg^{-1} K^{-1}) followed during isentropic expansion of vapor. For all interactions, water expands into the two-phase region. (b) A *T*–*S* diagram for pseudo-isothermal expansion shows the increase in entropy as water stays in thermal equilibrium with magma fragments. For R_r < 1.3 water expands into the vapor field. (c) A *p*–*T* diagram shows the variation in water temperature during pseudo-isothermal expansion. For more detail on these diagrams see Kieffer and Delany (1979).

~2.2 km ocean depth). However, the presence of other pressure perturbations, such as those caused by seismicity, host media failure, and the vapor-film dynamics, add to the likelihood that expansion will lead to thermohydraulic explosion.

11.4.3 A non-equilibrium thermodynamic model

In the supersonic explosive interaction regime (regime 3; Section 11.4.1), water reacts as a supercritical fluid that undergoes complex phase transitions that are difficult to model. Consequently, the steady-state models described in Section 11.4.2 do not fully capture some important physics. Experimental observations reveal that magma quenches with little or no phase change and can therefore be described as a supercooled liquid (i.e., glass; Section 11.3.2), the physical properties of which are well known and/or can easily be measured. It is therefore much simpler to model the non-equilibrium behavior of the magma rather than the complex phase reactions of the water.

The basis of the model is the heat conduction equation of standard, non-equilibrium thermodynamics applied to the individual magma fragments:

$$\frac{\partial T_{(x,y,z,t)}}{\partial t} = k_m \nabla^2 T_{(x,y,z,t)}, \qquad (11.13)$$

where $T_{(x,y,z,t)}$ is the time-dependent temperature-field inside the fragment and k_m is the thermal conductivity (approximately constant for supercooled liquids). The solution of this partial differential equation can be found in Büttner *et al.* (2005). Inserting the result into the heat flux equation yields:

$$\frac{\Delta Q_{(t)}}{\Delta t} = mc_m \frac{\Delta T_{(x,y,z,t)}}{\Delta t}, \qquad (11.14)$$

where $\Delta Q_{(t)}/\Delta t$ represents the time-dependent heat flux, m is the mass of the fragment, c_m is the specific heat capacity, and $\Delta T_{(x,y,z,t)}/\Delta t$ is the variation of the temperature field in the fragment with time. Analysis of experimentally produced particles yields the size, shape and number of particles produced for a given starting mass. Summing the heat transferred from all particles

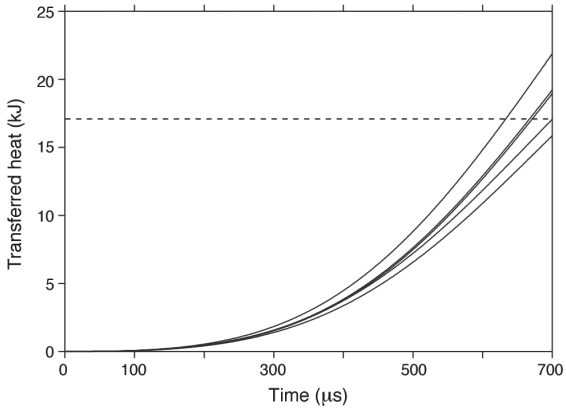

Figure 11.17 Results of heat flow modeling of a MFCI experiment, using the non-equilibrium thermodynamic approach. The different curves represent end members of fragment morphology (e.g., cubes, spheres), which show the limited influence of shape on the results. The dashed line represents the total measured heat transfer during the experiment, which ended in explosion after 700 μs. (After Büttner *et al.*, 2005.)

allows calculation of the total energy release and therefore the explosivity of this regime. Figure 11.17 shows the results of modeling the heat transfer during an MFCI experiment. The model curves predict well the total heat flow measured during the experiment (dashed line), confirming that this technique is robust with respect to the magma properties and fragment size and morphology. It is possible to extend this treatment to natural eruptions to evaluate the total energy release during explosive events by using grain size and shape analysis of natural tephra samples, together with appropriate magma properties and an assessment of the total mass of the deposit.

11.4.4 A brittle fragmentation model

The above non-equilibrium behavior is intimately tied to magma fragmentation by application of the Gibbs thermodynamic function (Yew and Taylor, 1994), which is expressed as:

$$G = U + B - TS, \tag{11.15}$$

where G is the Gibbs free energy, U is the pre-fragmentation internal energy of the magma, B is the surface energy consumed by fragmentation, and S is the entropy generated by creation of new surfaces during fragmentation. In order to apply this general function, one must assume:

(1) Magma breaks up due to internal stress (i.e., in a brittle regime);
(2) Thermodynamic equilibrium is not achieved during crack growth within the magma until its fragmentation into a number, n, of spherical particles;
(3) Isothermal conditions exist during fragmentation;
(4) Surface energy is not recoverable, and the entropy of the system increases; and
(5) During increments of time the stress is treated as constant.

Following the methods of Grady (1982, 1985), each term in Eq. (11.15) can be evaluated as follows. The value of U is taken as the strain energy in the magma just prior to failure, and it is a function of n, the number of particles formed by fragmentation:

$$U = \frac{\mu}{8}\left(\frac{\dot{\varepsilon}}{c}\right)^2 \left(\frac{6}{\pi}\right)^{2/3} n^{-2/3} V^{5/3}, \tag{11.16}$$

where μ is the magma bulk modulus ($\mu = \rho_m c^2$; ρ_m is density and c is sound speed), $\dot{\varepsilon}$ is the strain rate, and V is the total volume. Yew and Taylor (1994) give a simple geometric argument to constrain B, the total energy dissipated by fragmentation:

$$B = \left(\frac{\pi}{6}\right)^{1/3} \left(\frac{3K_c^2}{\rho_m c^2}\right) n^{1/3} V^{2/3}, \tag{11.17}$$

where K_c is the stress intensity factor. The entropy S of new surfaces can be evaluated by the configuration entropy of n cracks that could occupy $N + n$ sites in a volume V (Varotsos and Alexopoulos, 1986):

$$S = k_B \ln\left\{\frac{(N+n)!}{N!\,n!}\right\}, \tag{11.18}$$

where k_B is the Boltzmann constant and N is the total number of normalized new surfaces.

In order to apply Eq. (11.15) to the state where fragmentation has occurred, thermodynamic equilibrium is assumed at a constant

temperature and pressure where the Gibbs function is at a minimum:

$$\left(\frac{\partial G}{\partial n}\right)_{T,p} = 0. \tag{11.19}$$

By taking the derivative of Eq. (11.15), setting the average fragment size (s; Grady, 1982, 1985; Yew and Taylor, 1994) to:

$$s = \left(\frac{6V}{\pi n}\right)^{1/3} \approx 2\left[\frac{\sqrt{3}\,K_c}{\sqrt{2}\,\rho_m\, c\dot{\varepsilon}}\right]^{2/3}, \tag{11.20}$$

the strain rate associated with fragmentation that produces particulates of an average size s is expressed by:

$$\dot{\varepsilon} = \frac{K_c}{\rho c}\sqrt{\frac{12}{s^3}}. \tag{11.21}$$

The value of s can be constrained by inspection of tephra sample subpopulation modes, distinguished either by shapes and textures (e.g., Heiken and Wohletz, 1985, 1991) or by mode dispersion (e.g., Wohletz *et al.*, 1995b). Using an estimated stress intensity value K_c, fragmentation strain rates can be determined from Eq. (11.21). The strain rates are then related to E_f, the fragmentation energy, by:

$$E_f \approx \frac{1}{120}\left(\frac{6}{\pi}\right)^{2/3} \rho_m\, \dot{\varepsilon}\, n^{-2/3} V^{5/3}. \tag{11.22}$$

This treatment can be applied to natural hydrovolcanic deposits if the particle density and whole deposit volume and grain size distribution are known (see Büttner *et al.*, 2006, for details). Summation of the specific fragmentation energy for each grain size fraction and for the total deposit volume allows calculation of the total fragmentation energy for the eruption. Using an assessment of the partitioning of total eruption energy among fragmentation (50–75%), kinetic (15–30%), seismic (10–20%), and acoustic (<5%) energies, Büttner *et al.* (2006) calculated total eruption energies on the order 10^{14} J (~ 25 Mt of high explosive equivalent) for two eruptions at Campi Flegrei, Italy.

11.5 | Summary

The following points summarize a basic understanding of magma–water interactions during volcanism (hydrovolcanism). The numerous references cited in this chapter will permit the reader to gain a deeper appreciation of the physics of magma–water interaction.

- Magma–water interaction is not a rare process, and is relevant for nearly every volcanic system. Earth is a water planet and most of its volcanic activity is found underwater, especially at the mid-oceanic ridges (see Chapter 12).
- A well-developed catalog exists of diagnostics that are useful to characterize magma–water interaction from analysis of hydrovolcanic products, including vent/construct morphology, deposit dispersal, tephra bedding sequences, and ash analyses. However, a quantitative analysis in terms of energy balances and hazard mitigation needs experimental data and theoretical concepts.
- Whereas understanding of water physics is highly evolved because of the rich tradition of power plant technology, magma physics are less well understood, and volcanologists are just beginning to develop the complex physics needed to handle this multiphase, multicomponent, subliquidus system. Further data are required for basic physical parameters such as magma heat conductivity and viscosity, without which the dynamic heat transfer at the magma–water interface cannot be reliably quantified.
- The key process for understanding the energy balance of hydrovolcanism is magma fragmentation. To make the thermal energy available for conversion to mechanical energy via the working fluid water, heat must be transferred. Because heat transfer is dominated by conduction, the energy transfer rate increases with the increased surface area produced by fragmentation. Energy release on a short timescale (explosion) during hydrovolcanic processes is likely a result of a positive feedback mechanism in which heat exchange drives

fragmentation, which in turn drives escalating heat transfer rates.
- Three heat-flux regimes can be defined to cover the range of magma–water interaction dynamics from non-explosive passive cooling to supersonic thermal detonation. Modeling techniques comprise steady-state thermodynamics for the non-explosive to explosive interaction regimes, based on thermal power plant physics. Modeling of the supersonic explosive regime, however, benefits from application of non-equilibrium thermodynamics, which develops a strong link between explosion energy and fragment size distributions.

11.6 Notation

B	surface energy consumed by fragmentation (J)
c	sound speed (m s^{-1})
c_m	specific heat capacity of magma (J kg^{-1} K^{-1})
c_p	specific heat capacity at constant pressure (J kg^{-1} K^{-1})
c_r	specific heat capacity of saturated rock (J kg^{-1} K^{-1})
c_s	specific heat capacity of solids dissolved in water (J kg^{-1} K^{-1})
c_w	specific heat capacity of pure water (J kg^{-1} K^{-1})
E	mixture internal energy (J)
E_f	fragmentation energy (J)
G	Gibbs free energy (J)
k_B	Boltzmann constant ($1.3806488 \times 10^{-23}$ J kg^{-1})
k_m	thermal conductivity of magma (W m^{-1} K^{-1})
k_w	thermal conductivity of water (W m^{-1} K^{-1})
K_c	stress intensity factor (Pa $m^{1/2}$)
m	mass of particle (kg)
m_m	mass of magma (kg)
m_r	mass of porous rock (or impure water) (kg)
m_w	mass of water (kg)
n	number of particles produced by fragmentation event
N	number of new surfaces produced by fragmentation event
p	pressure (Pa)
p_{cj}	pressure at Chapman–Jouguet point (Pa)
R	mass ratio of water to magma
R_r	mass ratio of saturated rock (or impure water) to magma
Q	heat (J)
s	average fragment size (m)
S	entropy generated by fragmentation (J)
S_w	rock saturation (pore volume fraction filled with water)
t	time (s)
T	temperature (K)
T_e	equilibrium temperature (K)
T_I	instantaneous interface temperature (K)
T_m	magma temperature (K)
T_w	water temperature (K)
u	mixture velocity (m s^{-1})
u_r	velocity of shocked material relative to shock wave (m s^{-1})
U	internal energy of pre-fragmentation magma (J)
V	mixture volume (m^3) or specific volume (m^3 kg^{-1})
V_{cj}	volume at Chapman–Jouguet point (m^3)
V_m	volume of magma (m^3)
V_r	volume of porous rock or impure water (m^3)
V_w	volume of water (m^3)
W	thermodynamic work (J)
x_w	mass fraction of pure water
α	isobaric expansion coefficient (K^{-1})
β	isothermal expansion coefficient (Pa^{-1})
$\dot{\varepsilon}$	strain rate (s^{-1})
ϕ	porosity
$\dot{\gamma}$	shear rate (s^{-1})
η	dynamic viscosity (Pa s)
κ_m	thermal diffusivity of magma (m^2 s^{-1})
κ_w	thermal diffusivity of water (m^2 s^{-1})
μ	magma bulk modulus (Pa)
ν	dynamic viscosity (m^2 s^{-1})
ρ	mixture density (kg m^{-3})
ρ_m	magma density (kg m^{-3})
ρ_r	rock density (kg m^{-3})
ρ_w	water density (kg m^{-3})
ξ	ratio of water and magma specific heats

Acknowledgments

Much of this work was performed under the auspices of Los Alamos National Laboratory, operated by Los Alamos National Security, LLC for the National Nuclear Security Administration of the U.S. Department of Energy under contract DE-AC52–06NA25396.

References

Austin-Erickson, A., Büttner, R., Dellino, P., Ort, M. H., and Zimanowski, B. (2008). Phreatomagmatic explosions of rhyolitic magma: experimental and field evidence. *Journal of Geophysical Research*, **113**, B11201, doi:10.1029/2008JB005731

Baierlein, R. (1999). *Thermal Physics.* Cambridge University Press, 456 pp.

Bejan, A. and Eden, M. (1999). *Thermodynamic Optimization of Complex Energy Systems.* Springer.

Bischoff, J. L. and Rosenbauer, R. J. (1988). Liquid-vapor relations in the critical region of the system NaCl-H_2O from 380 to 415°C: a refined determination of the critical point and two-phase boundary of seawater. *Geochimica et Cosmochimica Acta*, **52**, 2121–2126.

Board, S. J., Farmer, C. L. and Poole, D. H. (1975). Fragmentation in thermal explosions. *Journal of Heat and Mass Transfer*, **17**, 331–339.

Bonatti, E. (1976). Mechanisms of deep sea volcanism in the South Pacific. In *Researches in Geochemistry 2*, ed. P. H. Ableson. New York: John Wiley & Sons, pp. 453–491.

Buchanan, D. J. (1974). A model for fuel-coolant interaction. *Journal of Physics D: Applied Physics*, **7**, 1441–1457.

Buchanan, D. J. and Dullforce, T. A. (1973). Mechanism for vapor explosions. *Nature*, **245**, 32–34.

Burnham, C. W., Holloway, J. R. and Davies, N. F. (1969). Thermodynamic properties of water to 1000°C and 10 000 bars. *Geological Society of America Special Paper*, **132**, 1–96.

Büttner, R. and Zimanowski, B. (1998). Physics of thermohydraulic explosions. *Physics Reviews E*, **57**(5), 5726–5729.

Büttner, R., Zimanowski, B., Blumm, J. and Hagemann, L. (1998). Thermal conductivity of a volcanic rock material (olivine-melilitite) in the temperature range between 288 and 1470 K. *Journal of Volcanology and Geothermal Research*, **80**, 293–302.

Büttner, R., Dellino, P. and Zimanowski, B. (1999). Identifying modes of magma/water interaction from the surface features of ash particles. *Nature*, **401**, 688–690.

Büttner, R., Zimanowski, B., Lenk, C., Koopmann, A. and Lorenz, V. (2000). Determination of thermal conductivity of natural silicate melts. *Applied Physics Letters*, **77**, 1810–1812.

Büttner, R., Dellino, P., LaVolpe, L., Lorenz, V. and Zimanowski, B. (2002). Thermohydraulic explosions in phreatomagmatic eruptions as evidenced by the comparison between pyroclasts and products from Molten Fuel Coolant Interaction experiments. *Journal of Geophysical Research*, **107**, doi: 10.1029/2001JB000792.

Büttner, R., Zimanowski, B., Mohrholz, C.-O. and Kümmel, R. (2005). Analysis of thermohydraulic explosion energetics. *Journal of Applied Physics*, **98**, 043524, doi:10.1063/1.2033149.

Büttner, R., Dellino, P., Raue, H., Sonder, I., and Zimanowski, B. (2006). Stress induced brittle fragmentation of magmatic melts: Theory and experiments. *Journal of Geophysical Research*, **111**, B08204, doi:101029/2005JB003958

Carlisle, D. (1963). Pillow breccias and their aquagene tuffs: Quadra Island, British Columbia. *American Journal of Science*, **71**, 48–71.

Corradini, M. L. (1981). Phenomenological modelling of the triggering phase of small-scale steam explosion experiments. *Nuclear Science and Engineering*, **78**, 154–170.

Courant, R. and Friedrichs, K. O. (1948). *Supersonic Flow and Shock Waves*. New York: Springer, 464 pp.

Cronenberg, A. W. (1980). Recent developments in the understanding of energetic molten fuel-coolant interactions. *Nuclear Safety*, **21**, 319–337

Delaney, P. T. (1982). Rapid intrusion of magma into wet rock: ground water flow due to pressure increases. *Journal of Geophysical Research*, **87**, 7739–7756.

Dellino, P., Isaia, R., La Volpe, L. and Orsi, G. (2001). Statistical analysis of textural data from complex pyroclastic sequences: Implications for fragmentation processes of the Agnano Monte Spina Tephra (4.1 ka), Phlegraean Fields, southern Italy. *Bulletin of Volcanology*, **63**, 443–461.

Drumheller, D. S. (1979). The initiation of melt fragmentation in fuel-coolant interactions. *Nuclear Science and Engineering*, **72**, 347–356.

Ebert, H.-P., Hernberger, F., Fricke, J. *et al.* (2003). Thermophysical properties of a volcanic rock material. *High Temperatures – High Pressures*, **34**, 561–668.

Fisher, R. V. and Schmincke, H.-U. (1984). *Pyroclastic Rocks*. Berlin: Springer-Verlag, 472 pp.

Fisher, R. V. and Waters, A. C. (1970). Base-surge bed forms in maar volcanoes. *American Journal of Science*, **268**, 157–180.

Frazzetta, G., La Volpe, L., and Sheridan, M. F. (1983). Evolution of the Fossa cone, Vulcano. *Journal of Volcanology and Geothermal Research*, **17**, 329–360.

Fuller, R. E. (1931). The aqueous chilling of basaltic lava on the Columbia River Plateau. *American Journal of Science*, **21**, 281–300.

Grady, D. E. (1982). Local inertial effects in dynamic fragmentation. *Journal of Applied Physics*, **53**, 322–523.

Grady, D. E. (1985). Fragmentation under impulsive stress loading. In *Fragmentation by Blasting*, ed. W. L. Fourney and R. R. Boade. Society for Experimental Mechanics, Brookfield Center, 63–72.

Greer, S. C. and Moldover, M. R. (1981). Thermodynamic anomalies at critical points of fluids. *Annual Reviews of Physical Chemistry*, **32**, 233–265.

Heiken, G. (1971). Tuff rings: examples from the Fort Rock-Christmas Lake Valley, south-central Oregon. *Journal of Geophysical Research*, **76**, 5615–5626.

Heiken, G. and Wohletz, K. H. (1985). Volcanic Ash. Berkely, CA: University of California Press, 245 pp.

Heiken, G. and Wohletz, K. (1991). Fragmentation processes in explosive volcanic eruptions. In *Sedimentation in Volcanic Settings*, ed. R. V. Fisher and G. Smith, Society of Sedimentary Geology Special Publication **45**, 19–26.

Henry, R. E. and Fauske, H. K. (1981). Required initial conditions for energetic steam explosions. In *Fuel–Coolant Interactions*. New York: American Society of Mechanical Engineers, Report HTD-V19.

Herrmann, H. J. and Roux, S. (1990). *Statistical Models for the Fracture of Disordered Media*, Amsterdam: North Holland.

Holloway, J. R. (1977). Fugacity and activity of molecular species in supercritical fluids. In *Thermodynamics in Geology*, ed. D. G, Fraser. Dordrecht, Holland: Reidel, pp. 161–181.

Honnorez, H. and Kirst, P. (1975). Submarine basaltic volcanism: morphometric parameters for discriminating hyaloclastites from hyalotuffs. *Bulletin of Volcanology*, **39**, 441–465.

Jaggar, T. A. (1949). Steam blast volcanic eruptions. Hawaii Volcano Observatory, 4th Special Report.

Kieffer, S. W. and Delany, J. M. (1979). Isentropic decompression of fluids from crustal and mantle pressures. *Journal of Geophysical Research*, **84**, 1611–1620.

Kokelaar, P. (1986). Magma-water interactions in subaqueous and emergent basaltic volcanism. *Bulletin of Volcanology*, **48**, 275–290.

Krauskopf, K. B. (1967). *Introduction to Geochemistry*. New York: McGraw-Hill.

Landau, L. D. and Lifshitz, B. M. (1959). *Fluid Mechanics: Volume 6, Course of Theoretical Physics*. New York: Pergamon.

Mastin, L. G. (2007). Generation of fine hydromagmatic ash by growth and disintegration of glassy rinds. *Journal of Geophysical Research*, **112**, B02203, doi:10.1029/2005JB003883.

Moore, J. G., Nakamura, K. and Alcaraz, A. (1966). The 1965 eruption of Taal Volcano. *Science*, **151**, 995–960.

Morrissey, M., Zimanowski, B., Wohletz, K., and Büttner, R. (2000). Phreatomagmatic Fragmentation. In *Encyclopedia of Volcanism*, ed. H. Sigurdsson. London: Academic Press, pp. 431–445.

Muffler, L. J. P., White, D. E. and Truesdell, A. H. (1971). Hydrothermal explosion craters in Yellowstone National Park. *Geological Society of America Bulletin*, **82**, 723–740.

Nairn, I. A. and Solia, W. (1980). Late Quaternary hydrothermal explosion breccias at Kawerau geothermal field, New Zealand. *Bulletin of Volcanology*, **43**, 1–13.

Noe-Nygaard, A. (1940). Subglacial volcanic activity in ancient and recent times. *Folia Geograph. Danica*, **1**, no. 2.

Ollier, C. D. (1974). Phreatic eruptions and maars. In *Physical Volcanology*, ed. L. Civett, P. Gasparini, G. Luongo, and A. Rapolla. New York: Elsevier, 289–310.

Ruggles, A E., Drew, D. A., Lahey, R. T., Jr. and Scarton, H. A. (1989). The relationship between standing waves, pressure pulse propagation and the critical flow rate in two-phase mixtures. *Journal of Heat Transfer*, **111**, 467–473.

Ruggles, A. E., Vasiliev, A. D., Brown, N. W. and Wendel, M. W. (1997). Role of heater thermal response in reactor thermal limits during oscillatory two-phase flows. *Nuclear Science and Engineering*, **125**, 75–83.

Schmid, A., Sonder, I., Seegelken, R. *et al.* (2010). Experiments on the heat discharge at the dynamic

magma-water-interface. *Geophysical Research Letters*, **37**, L20311, doi: 10.1029/2010GL044963

Self, S., Kienle, J. and Huot, J.-P. (1980). Ukinrek maars, Alaska, II. Deposits and formation of the 1977 craters. *Journal of Volcanology and Geothermal Research*, **7**, 39–65.

Servicos Geologicos de Portugal (1959). Le volcanisme de l'isle de Faial et l'éruption de volcan de Capelinhos. *Memorandum* **4**, 100 pp.

Sheridan, M. F. and Wohletz, K. H. (1983). Hydrovolcanism: basic considerations and review. *Journal of Volcanology and Geothermal Research*, **17**, 1–29.

Sigvaldason, G. (1968). Structure and products of subaquatic volcanoes in Iceland. *Contributions to Mineralogy and Petrology*, **18**, 1–16.

Sonder, I., Büttner, R. and Zimanowski, B. (2006). Non-Newtonian viscosity of basaltic magma. *Geophysical Research Letters*, **33**, L02303, doi:10.1029/2005GL024240.

Sonder, I., Schmid, A., Seegelken, R., Zimanowski, B. and Büttner, R. (2011). Heat source or heat sink: What dominates behavior of non-explosive magma-water interaction? *Journal of Geophysical Research*, **116**, B09203, doi:10.1029/2011JB008280.

Sourirajan, S. and Kennedy, G. C. (1962). The system H_2O-NaCl at elevated temperatures and pressures. *American Journal of Science*, **260**, 115–141.

Tazieff, H. K. (1958). L'éruption 1957–1958 et la tectonique de Faial (Azores). *Annales de la Sociéte Géologique de Belgique*, **67**, 14–49.

Theofanous, T. G. (1995). The study of steam explosion in nuclear systems. *Nuclear Engineering Design*, **155**, 1–26.

Thorarinsson, S. (1964). *Surtsey, the new island in the North Atlantic*. Reykjavik: Almenna Bokofelagid.

Turekian, K. K. (1968). *Oceans*. New Jersey: Prentice-Hall, 150 pp.

Varotsos, P. A. and Alexopoulos, K. D. (1986). *Thermodynamics of Point Defects and Their Relation with Bulk Properties*. Amsterdam: North-Holland.

Waters, A. C. and Fisher, R. V. (1971). Base surges and their deposits: Capelinhos and Taal Volcanoes. *Journal of Geophysical Research*, **76**, 5596–5614.

Wentworth, C. K. (1938). *Ash formations of the island of Hawaii*. Hawaii Volcano Observatory, 3rd Special Report. Honolulu: Hawaiian Volcano Research Society, 173 pp.

White, J. D. L. (1996). Impure coolants and interaction dynamics of phreatomagmatic eruptions. *Journal of Volcanology and Geothermal Research*, **74**, 155–170.

Wohletz, K. H. (1983). Mechanisms of hydrovolcanic pyroclast formation: grain-size, scanning electron microscopy, and experimental results. *Journal of Volcanology and Geothermal Research*, **17**, 31–63.

Wohletz, K. H. (1986). Explosive magma-water interactions: thermodynamics, explosion mechanisms, and field studies. *Bulletin of Volcanology*, **48**, 245–264.

Wohletz, K. H. (1987). Chemical and textural surface features of pyroclasts from hydrovolcanic eruption sequences. In *Clastic Particles,* ed. J. R. Marshall. New York: Van Nostrand Reinhold, pp. 79–97.

Wohletz, K. H. (1993). Hidrovolcanismo. In *Nuevas Tendencias: La Volcanologia Actual,* ed. J. Martí and V. Araña. Madrid: Consejo Superior de Investigaciones Cientificas, pp. 99–196.

Wohletz, K. H. (2003). Water/magma interaction: physical considerations for the deep submarine environment. In: *Submarine Explosive Volcanism,* American Geophysical Union Monograph **140**, 25–49.

Wohletz, K. H. and Heiken, G. (1992). *Volcanology and Geothermal Energy*. Berkely, CA: University of California Press.

Wohletz, K. H. and McQueen R. G. (1984). Experimental studies of hydromagmatic volcanism. In *Explosive Volcanism: Inception, Evolution, and Hazards*. Washington: National Academy Press, 158–169.

Wohletz, K. H. and Sheridan, M. F. (1983). Hydrovolcanic explosions II. Evolution of basaltic tuff rings and tuff cones. *American Journal of Science* **283**, 385–413.

Wohletz, K. H., McQueen, R. G. and Morrissey, M. (1995a). Analysis of fuel-coolant interaction experimental analogs of hydrovolcanism. In *Intense Multiphase Interactions,* ed. T. G. Theofanous and M. Akiyama. Proceedings of US (NSF) Japan (JSPS) Joint Seminar, Santa Barbara, CA, pp. 287–317.

Wohletz, K. H., Orsi, G. and de Vita, S. (1995b). Eruptive mechanisms of the Neapolitan Yellow Tuff interpreted from stratigraphy, chemistry, and granulometry. *Journal of Volcanology and Geothermal Research*, **67**, 263–290.

Yew, C. H. and Taylor, P. A. (1994). A thermodynamic theory of dynamic fragmentation. *International Journal of Impact Engineering*, **15**, 385–394.

Yuen, W. W. and Theofanous, T. G. (1994). The prediction of 2D thermal detonations and resulting damage potential. *Nuclear Engineering Design*, **155**, 289–309.

Zel'dovich, Ya. B. and Kompaneets A. S. (1960). *Theory of Detonation.* London: Academic Press.

Zel'dovich, Ya. B. and Raizer, Yu. P. (1966). *Physics of Shock Waves and High-Temperature Hydrodynamic Phenomena*, Volumes I and II. New York: Academic Press.

Zimanowski, B. (1998). Phreatomagmatic explosions. In *From Magma to Tephra,* ed. A. Freundt and M. Rosi. Developments in Volcanology **4**, Amsterdam: Elsevier, pp. 25–54.

Zimanowski, B. and Büttner, R. (2002). Dynamic mingling of magma and liquefied sediments. In *Peperite,* ed. I. Skilling, J. D. L. White and J. McPhie. Amsterdam: Elsevier, pp. 37–44.

Zimanowski, B. and Büttner, R. (2003). Phreatomagmatic explosions in subaqueous eruptions. In *Explosive Subaqueous Volcanism,* ed. J. D. L. White, J. L. Smellie and D. Clague. American Geophysical Union Monograph **140**. Washington, pp. 51–60.

Zimanowski, B., Fröhlich, G. and Lorenz, V. (1991). Quantitative experiments on phreatomagmatic explosions. *Journal of Volcanology and Geothermal Research*, **48**, 341–358.

Zimanowski, B., Büttner, R., Lorenz, V. and H.-G., Häfele (1997a). Fragmentation of basaltic melt in the course of explosive volcanism. *Journal of Geophysical Research*, **107**, 803–814.

Zimanowski, B., Büttner, R. and Nestler, J. (1997b). Brittle reaction of a high temperature ion melt. *Europhysics Letters*, **38**, 285–289.

Zimanowski, B., Wohletz, K. H., Büttner, R. and Dellino, P. (2003). The volcanic ash problem. *Journal of Volcanology and Geothermal Research*, **122**, 1–5.

Online resources available at www.cambridge.org/fagents

- Supplement 11A: Calculation of interaction thermodynamic work
- Supplement 11B: Video of MFCI experiments
- Links to websites of interest